ARMY RESEARCH LABORATORY

ARL

Modeling Finite Deformations in Trigonal Ceramic Crystals with Lattice Defects

by J. D. Clayton

NOTICES

Disclaimers

The findings in this report are not to be construed as an official Department of the Army position unless so designated by other authorized documents.

Citation of manufacturer's or trade names does not constitute an official endorsement or approval of the use thereof.

Destroy this report when it is no longer needed. Do not return it to the originator.

Army Research Laboratory
Aberdeen Proving Ground, MD 21005

Modeling Finite Deformations in Trigonal Ceramic Crystals with Lattice Defects

J. D. Clayton
Weapons and Materials Research Directorate, ARL

REPORT DOCUMENTATION PAGE

1. REPORT DATE (DD-MM-YYYY)	2. REPORT TYPE	3. DATES COVERED (From - To)
August 2010	Reprint	January 2009 - January 2010

4. TITLE AND SUBTITLE	5a. CONTRACT NUMBER
Modeling Finite Deformations in Trigonal Ceramic Crystals with Lattice Defects	
	5b. GRANT NUMBER
	5c. PROGRAM ELEMENT NUMBER

6. AUTHOR(S)	5d. PROJECT NUMBER
J. D. Clayton	AH80
	5e. TASK NUMBER
	5f. WORK UNIT NUMBER

7. PERFORMING ORGANIZATION NAME(S) AND ADDRESS(ES)	8. PERFORMING ORGANIZATION REPORT NUMBER
U.S. Army Research Laboratory ATTN: RDRL-WMT-D 2800 Powder Mill Road Adelphi, MD 20783-1197	ARL-RP-0297

9. SPONSORING/MONITORING AGENCY NAME(S) AND ADDRESS(ES)	10. SPONSOR/MONITOR'S ACRONYM(S)
	11. SPONSOR/MONITOR'S REPORT NUMBER(S)

12. DISTRIBUTION/AVAILABILITY STATEMENT

Approved for public release; distribution unlimited.

13. SUPPLEMENTARY NOTES

14. ABSTRACT

A model is developed for thermomechanical behavior of defective, low-symmetry ceramic crystals such as α-corundum. Kinematics resolved are nonlinear elastic deformation, thermal expansion, dislocation glide, mechanical twinning, and residual lattice strains associated with eigen stress fields of defects such as dislocations and stacking faults. Multiscale concepts are applied to describe effects of twinning on effective thermoelastic properties. Glide and twinning are thermodynamically irreversible, while free energy accumulates with geometrically necessary dislocations associated with strain and rotation gradients, statistically stored dislocations, and twin boundaries. The model is applied to describe single crystals of corundum. Hardening behaviors of glide and twin systems from the total density of dislocations accumulated during basal slip are quantified for pure and doped corundum crystals. Residual lattice expansion is predicted from nonlinear elasticity and dislocation line and stacking fault energies.

15. SUBJECT TERMS

Alumina, ceramic, elasticity, plasticity, twinning, defects

16. SECURITY CLASSIFICATION OF:			17. LIMITATION OF ABSTRACT	18. NUMBER OF PAGES	19a. NAME OF RESPONSIBLE PERSON
a. REPORT	b. ABSTRACT	c. THIS PAGE	UU	36	J. D. Clayton
Unclassified	Unclassified	Unclassified			19b. TELEPHONE NUMBER (Include area code) (410) 278-6146

Modeling finite deformations in trigonal ceramic crystals with lattice defects ☆

J.D. Clayton

Impact Physics, U.S. Army Research Laboratory, Aberdeen Proving Ground, MD 21005-5066, USA

ABSTRACT

A model is developed for thermomechanical behavior of defective, low-symmetry ceramic crystals such as α-corundum. Kinematics resolved are nonlinear elastic deformation, thermal expansion, dislocation glide, mechanical twinning, and residual lattice strains associated with eigenstress fields of defects such as dislocations and stacking faults. Multiscale concepts are applied to describe effects of twinning on effective thermoelastic properties. Glide and twinning are thermodynamically irreversible, while free energy accumulates with geometrically necessary dislocations associated with strain and rotation gradients, statistically stored dislocations, and twin boundaries. The model is applied to describe single crystals of corundum. Hardening behaviors of glide and twin systems from the total density of dislocations accumulated during basal slip are quantified for pure and doped corundum crystals. Residual lattice expansion is predicted from nonlinear elasticity and dislocation line and stacking fault energies.

Published by Elsevier Ltd.

1. Introduction

By standard definition, a ceramic crystal is an inorganic, non-metallic, ordered solid. Electronic structures of ceramics feature ionic and/or covalent bonds rather than metallic bonds found in ductile metals. The nature of inter-atomic forces in ceramics often correlates with a high Peierls barrier (Peierls, 1940; Nabarro, 1947; Friedel, 1964), inhibiting dislocation motion at low temperatures and leading to brittleness, i.e., a tendency towards fracture over slip.

Anisotropic and non-cubic crystals are of particular interest in the present work. In certain hexagonal ceramics such as silicon carbide (Zhang et al., 2005), basal slip is often the preferred inelastic deformation mechanism, with slip resistances extremely high in directions normal to the basal plane. This phenomenon occurs similarly in many hexagonal metals, including certain alloys of zirconium (Tomé et al., 1991a; McCabe et al., 2009), titanium (Schoenfeld and Kad, 2002; Mayeur and McDowell, 2007), and magnesium (Staroselsky and Anand, 2003; Neil and Agnew, 2009), though in some cases pyramidal slip modes are possible. Deformation twinning, as opposed to slip, is often the only viable mechanism for accommodating deformation normal to the basal plane, in lieu of fracture. Twinning is often favored over slip in cubic metals with low stacking fault energies (Christian and Mahajan, 1995; Kalidindi, 1998, 2001); twinning may also influence shear band formation in cubic metals (Paul et al., 2009). In addition to silicon carbide, other low-symmetry ceramics of interest for high rate applications, because of their hardness and dynamic compressive strength, include titanium diboride (Bourne and Gray, 2002) and alumina (Bourne, 2006; Bourne et al., 2007).

At low temperatures and pressures, the stable phase of single crystalline alumina (Al_2O_3) is α-corundum. Although other phases exist (Holm et al., 1999), henceforth the term corundum will refer only to the α phase. The Bravais lattice is

---

rhombohedral (i.e., trigonal), though the unit cell is often described via hexagonal notation (Kronberg, 1957; Snow and Heuer, 1973). Corundum is centrosymmetric and hence not piezoelectric. Corundum that is red in color, for example resulting from chromium doping, is commonly called ruby (Chang, 1960; Klassen-Neklyudova et al., 1970; Inkson, 2000). Corundum of all other colors is often referred to as sapphire, with blue sapphire containing trace amounts of cobalt, titanium, or iron, for example. Corundum is extremely hard, with a value of 9 on Mohr's scale, and exhibits a very high Hugoniot Elastic Limit (HEL, the usual measure of dynamic yield strength under uniaxial strain conditions, at high pressure), with values in excess of 20 GPa for single crystals of certain orientations (Graham and Brooks, 1971). Single crystals of adequate purity are transparent, with uses in optics and electronics. However, the HEL and toughness of commercial grade, polycrystalline alumina are lower than that of single crystalline corundum, often thought a result of porosity and amorphous phases in the vicinity of grain boundaries (Bourne et al., 2007). Industrial-grade polycrystalline alumina manufactured by sintering is generally not transparent.

The present study focuses on mechanisms of elasticity, plastic slip, and deformation twinning. Each mechanism is addressed independently via an individual term within a three-term multiplicative decomposition of the deformation gradient (Kratochvil, 1972; Clayton et al., 2005). According to this representation, plastic deformation is deemed lattice-preserving (i.e., dislocation glide does not affect the lattice vectors or stored elastic energy of crystal), following Bilby et al. (1957), who introduced a two-term multiplicative decomposition for describing elasticity and plasticity of crystalline solids subjected to large deformations. In contrast, twinning is modeled here distinctly from dislocation plasticity via the use of an isochoric intermediate term in the deformation gradient decomposition, following Kratochvil (1972), Clayton et al. (2005), who used intermediate terms within three-term decompositions to account for irreversible deformations that are not lattice-preserving. Microscopic strain fields associated with defects in the lattice may also contribute to the intermediate deformation mapping. Here, isotropic contributions of the local fields follow from multiscale volume averaging and nonlinear elastic analysis of self-equilibrated bodies with defects (Seeger and Haasen, 1958; Toupin and Rivlin, 1960; Teodosiu, 1982; Wright, 1982; Clayton and Bammann, 2009). Following the theory of continuum crystal plasticity (Hutchinson, 1976; Teodosiu and Sidoroff, 1976; Asaro, 1983), plastic deformation takes place via slip on one or more discrete systems. Twinning takes place via energy invariant shears of predefined magnitude, with the rate of shearing determined by the rate of increase in volume fraction of the twin relative to the parent (Chin et al., 1969; Van Houtte, 1978; Staroselsky and Anand, 2003). Thermodynamically reversible deformation of the lattice is addressed via the elastic term in the decomposition, encompassing recoverable deformation associated with mechanical stress and stress-free thermal expansion/contraction. Multiscale averaging concepts are invoked to describe effects of twinning on the thermoelastic response, leading to effective anisotropic elastic coefficients and dissipation rates that evolve in conjunction with the volume fractions of twins in an element of fixed mass in the crystal.

A constitutive framework based on internal state variable theory provides thermodynamic relationships among independent and dependent state variables as well as appropriate driving forces for evolution of internal variables and rates of inelastic deformations. Here, the former consist of dislocation and twin boundary densities, and the latter include rates of slip and of twinned volumes. Dislocation densities consist of geometrically necessary dislocations associated with slip gradients (Nye, 1953; Ashby, 1970; Fleck et al., 1994; Arsenlis and Parks, 1999; Rezvanian et al., 2007) and statistically stored dislocations associated with homogeneous plastic flow and dislocation loops (Ashby, 1970; Arsenlis and Parks, 1999; Rezvanian et al., 2007). Interface partial dislocations at propagating twin boundaries (Scott and Orr, 1983) are demonstrated to also contribute to the geometrically necessary dislocation density tensor, following kinematic arguments regarding inelastic deformation incompatibility in plastically deformed single crystals (Clayton et al., 2004a,b). Thermodynamic restrictions on kinetic relations follow naturally from energy conservation requirements and the entropy inequality (Eckart, 1948; Coleman and Gurtin, 1967; Teodosiu, 1970; McDowell, 2005). Defects in corundum are known to contribute to lattice curvature (Nye, 1953) and work hardening (Klassen-Neklyudova et al., 1970; Pletka et al., 1977, 1982).

The theoretical model formalized here can be used to represent corundum single crystals within an aggregate of polycrystalline alumina, for example in mesoscale numerical simulations (Bourne, 2006) of grain interactions, stress wave propagation, and defects. Additionally, the model may enable refinement of macroscopic continuum models used in engineering design (Rajendran, 1994), providing insight into important mechanisms occurring at the scale of individual grains.

The present application focuses on alumina because of the availability of experimental data quantifying the mechanical (i.e., stress-deformation) response of single crystals of various orientations across a wide range of temperatures and strain rates (Graham and Brooks, 1971; Tymiak and Gerberich, 2007; Rodriguez et al., 2008). While various kinetic relationships for slip (Lagerlof et al., 1994) and twinning (Scott and Orr, 1983) have been posited to describe the results of specific experiments, a more general continuum model is needed to collectively explain the behavior of corundum over a range of loading conditions.

In a previous paper (Clayton, 2009), a theoretical model was developed to address anisotropic nonlinear elasticity, slip, and twinning in pure sapphire. The focus of that investigation centered on the shock response of oriented single crystals subjected to uniaxial strain, with results of nonlinear elastic calculations combined with experimental HEL data to provide bounds on critical stresses for dislocation glide and twin nucleation. Here, that theoretical model is extended to delineate geometrically necessary dislocations resulting from gradients of inelastic stretch and rotation (i.e., deformation incompatibility) as well as statistically stored dislocations associated with dislocation dipoles and loops, for example. Inclusion of geometrically necessary dislocations requires introduction of a length scale (Fleck et al., 1994; Regueiro et al., 2002) in the thermodynamic framework and renders the model nonlocal according to many labeling schemes. The application in the

present paper focuses on strain hardening, defect accumulation, and stored energy of defects in doped corundum, in addition to the pure sapphire considered previously. A more extensive treatment of volume changes resulting from eigenstress fields of defects is also given here, including predictions for volume changes resulting from twin boundary energies.

This paper is organized as follows. In Section 2, physical descriptions of elasticity, plasticity, and twinning are provided, in a more extensive treatment than given previously (Clayton, 2009). The descriptions serve to distinguish among the three deformation mechanisms and provide sufficient physical basis for the corresponding theoretical framework that follows in Section 3. The framework of Section 3 is generic enough to apply to any crystalline solid that undergoes large deformations via elasticity, plasticity, and/or twinning, including metallic and ceramic crystals. In Section 4, the model is specialized to describe the behavior of corundum single crystals. Section 4 begins with a review of the crystal structure of corundum (i.e., atomic positions, lattice parameters, and slip and twinning systems) and its fundamental physical properties. Hardening behaviors of glide and twin systems from the density of dislocations accumulated during basal slip observed in experiments on pure alumina (Pletka et al., 1977; Castaing et al., 2002) and corundum doped with Cr, Mg, or Ti cations (Pletka et al., 1982) are addressed. Stored residual energies associated with stress fields of dislocations, stacking faults, and twin boundaries are quantified. Residual elastic volume changes in pure and doped corundum are predicted from nonlinear elasticity theory and dislocation line and stacking fault energies. New comparisons of model predictions for rhombohedral twinning with experiments (Scott and Orr, 1983; Castaing et al., 2002) are provided. Finally, comparisons of model features (e.g., basal glide resistance, basal dislocation energy, and expansion associated with basal stacking faults) with results of atomic simulations performed elsewhere (Marinopoulos and Elsasser, 2001; Bodur et al., 2005; Zhang et al., 2007, 2008; Nishimura et al., 2009) are reported. The present paper is self-contained; hence, some overlap of material in Sections 3 and 4 with content of a previous paper (Clayton, 2009) is inevitable because all definitions of mathematical symbols and values of material properties entering the present, more refined theoretical model and application are included here for completeness. Differences in theory and results from the previous paper (Clayton, 2009) are highlighted as they appear.

The following notation is used. Scalars and individual components of vectors and tensors are written in italic font, while vectors and tensors are written in bold font. Einstein's summation convention applies for repeated indices. The $\cdot$ symbol denotes the scalar product of vectors ($\mathbf{a} \cdot \mathbf{b} = a^a b_a = a^1 b_1 + a^2 b_2 + a^3 b_3$), while $\otimes$ indicates the outer product ($(\mathbf{a} \otimes \mathbf{b})^{ab} = a^a b^b$). Juxtaposition of second-rank tensors implies summation over one set of adjacent indices ($(\mathbf{AB})^a_{\cdot c} = A^{ab} B_{bc}$). Summation over two sets of adjacent indices is denoted: ($\mathbf{A} : \mathbf{B} = A^{ab} B_{ab}$). Indices in parentheses are symmetric ($2A_{(ab)} = A_{ab} + A_{ba}$); indices in braces are skew ($2A_{[ab]} = A_{ab} - A_{ba}$). Superposed $\cdot$, T, and -1 denote material time differentiation, transposition, and inversion, respectively, and subscripted commas denote partial differentiation.

2. Background: deformation mechanisms

2.1. Elasticity

A crystal is said to deform elastically in the absence of generation or motion of defects. At the atomic scale, elastic deformation alters relative distances and/or orientations among neighboring atoms within each crystallographic unit cell. Resulting changes in inter-atomic forces produce mechanical stress when the crystal is viewed as a continuous solid. Removal of mechanical stresses restores the original inter-atomic bond lengths and angles without dissipation of energy; hence, elastic deformation is said to be thermodynamically reversible. Here, elastic deformation also includes changes in average inter-atomic bond vectors induced by changes in temperature. Increases in thermal energy, i.e., local atomic vibrations, usually correlate with expansion of the lattice in the absence of mechanical stresses. Such thermal deformations are deemed reversible, since atomic nuclei will return to their mean reference positions as the temperature is restored to its original value. Let $\mathbf{F}^E$ denote the two-point tensor of possibly large elastic deformation. Let $\mathbf{a}_0$ denote the vector between sites in a conventional unit cell such that $a_0 = (\mathbf{a}_0 \cdot \mathbf{a}_0)^{1/2}$ is a conventional lattice parameter. Primitive Bravais lattice vectors and conventional lattice vectors deform via the elastic deformation according to the Cauchy–Born hypothesis (Born and Huang, 1954; Ericksen, 1984). This is written $\mathbf{a} = \mathbf{F}^E \mathbf{a}_0$, with $\mathbf{a}$ the conventional lattice vector in the deformed crystal. An elastic deformation by simple shear of a non-cubic lattice is shown in Fig. 1(a). In the present description, electric polarization and relative internal
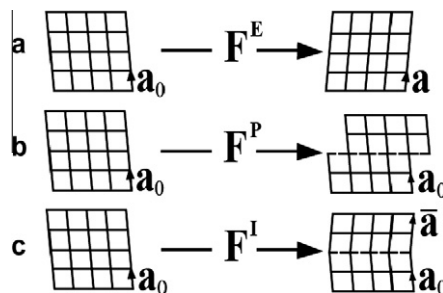

Fig. 1. Deformation mechanisms and lattice vectors: (a) elasticity, (b) slip, and (c) twinning.

shifts between sub-lattices in non-centrosymmetric crystals (Born and Huang, 1954; Cousins, 1978) are not addressed explicitly; rather, elastic deformation of a volume element is uniform over all inter-atomic bond vectors within that element.

2.2. Plasticity

Plastic deformation as defined here takes place via glide of dislocations of edge, screw, and/or mixed character, including loops, and encompassing cross-slip but not climb, the latter which requires further generalization (McDowell and Mooseb-rugger, 1992). As full dislocations travel through a region of the crystal, the shape of the material will change, but inter-atomic distances remain the same, so long as no defects are left behind in that region. In this sense, plastic deformation is said to be lattice-preserving or "lattice invariant" (Bilby et al., 1957). Mechanical stresses are conventionally required to enact the net glide of dislocations (apart from random thermal fluctuations). For example, resolved shear stresses must exceed the Peierls barrier in the context of lattice statics or Schmid's limit in the context of continuum slip (Hirth and Lothe, 1982). Plastic deformation is thermomechanically irreversible, since the reference shape of the material is not recovered upon removal of mechanical stresses, and since heat is dissipated by moving dislocations as a result of lattice friction, pho-non drag, and other mechanisms (Kocks et al., 1975; Gilman, 1979). Because the lattice remains unchanged apart from steps on the surface of the crystal, plastic deformation itself does not affect the strain energy of the crystal. However, defects gen-erated during plastic deformation that remain within the material lead to energy storage as a result of local stress fields in-duced by these defects and their core energies. Let $\mathbf{F^P}$ denote the two-point tensor of possibly large plastic deformation. Plastic deformation by simple shear is illustrated for a non-cubic lattice in Fig. 1(b). Lattice vector $\mathbf{a}_0$ is unchanged by the plastic deformation.

2.3. Twinning

Deformation twinning results in two connected regions in the lattice separated by a twin boundary (i.e., the habit plane or dotted line on the right side of Fig. 1(c)) whose shape deformations differ by a simple shear. The original lattice is termed the "parent", while the sheared lattice is termed the "twin". Atomic positions, and hence corresponding bond vectors between these atoms, within each region differ by a finite rotation, typically either a reflection or 180° rotation (Christian and Maha-jan, 1995), though more general relationships are possible. The stacking sequence of atomic planes in the twin is altered with respect to that in the parent, and hence crystals with low stacking fault energies are often more prone to twinning than those with high stacking fault energies. Nucleation and propagation of deformation twins are thought to take place by one or more mechanisms, often involving formation and motion of partial dislocations (e.g., dissociation of full dislocations into partials) and atomic shuffles sometimes needed to maintain orientation relationships between twin and parent (Bilby and Crocker, 1965; Zanzotto, 1996). Thus, twinning is not regarded as lattice-preserving in the sense of slip, since twinning involves rota-tion of the lattice, as evidenced by texture measurements (Van Houtte, 1978; Tomé et al., 1991a). Involvement of partial dis-locations and atomic shuffles induces the rotational change of the twinned lattice relative to that of the parent. Deformation twinning is also distinguished from plastic slip in that the former occurs by collective motion of defects, resulting in a quan-tized amount of shear that preserves the particular orientation relationship between the twin and parent. In contrast, plastic deformation may result in shearing of any magnitude, with the lower limit of relative displacement of atomic planes asso-ciated with the Burgers vector for slip. The shear strain associated with twinning is deemed mechanically irreversible, since twins considered here remain in single crystals after mechanical stresses are removed. Another difference between slip and twinning is that twinning is polar (i.e., unidirectional) while often slip is not. Lattice geometry precludes twinning shears of equal magnitude and opposite directions on the same plane, while typically slip may occur in opposite directions on the same plane, though resistances to slip in opposite directions on the same plane may differ (Lee et al., 1999; Xu et al., 2004).

Unstressed twinned regions of the crystal far from internal boundaries or defects possess the same strain energy density as the unstressed parent (James, 1981; Zanzotto, 1996); hence, twinning shears are said to be energy invariant. However, the energy density increases relative to that of a perfect lattice in the vicinity of twin boundaries (e.g., appropriate stacking fault energies). The mechanical work done during deformation twinning is dissipative, resulting from the defect motion (e.g., par-tial dislocation glide) associated with shearing. Possible energy storage is associated only with defects left behind in the crys-tal, for example those comprising the twin boundary. From continuum thermomechanics considerations, the driving force for twin propagation is the resolved shear stress in the direction of twinning shear. The resistance to deformation twinning is often modeled analogously to slip, that is, twinning proceeds when the resolved stress attains a critical value that may depend on temperature (Lagerlof et al., 1994; Wu et al., 2007). With accumulated slip and deformation twinning, strain hard-ening of the crystal may take place via interactions among different twins in the crystal, interactions among different slip systems, and interactions between mobile dislocations and twins (e.g., twin boundaries may serve as barriers to dislocation glide). Twins may also nucleate cracks and vice-versa (Christian and Mahajan, 1995). Detwinning, i.e., restoration of the twinned lattice to its original orientation, is physically possible, though is often more applicable to phase transformation phenomena (Bhattacharya, 1991; Thamburaja et al., 2009) and less applicable to mechanical twinning in the context of mon-atomic loading. In certain metals such as Mg alloys, however, deformation-induced detwinning can be important, especially during load sequences involving strain path changes (Proust et al., 2009).

Twins are usually classified as type I, type II, or compound. In centrosymmetric crystals, Bravais lattice vectors in the twin and parent for a type I twin are related by either a reflection in the habit plane or rotation of 180° about the direction normal

to this plane. For a type II twin, lattice vectors are related by either a rotation of 180° about the shear direction or a reflection in the plane normal to the shear direction. In crystals with a center of symmetry, the rotation (Van Houtte, 1978; Christian and Mahajan, 1995)

$$\overline{\mathbf{Q}} = \begin{cases} 2\mathbf{m}_0 \otimes \mathbf{m}_0 - \mathbf{1} \ (\text{type I}), \\ 2\mathbf{s}_0 \otimes \mathbf{s}_0 - \mathbf{1} \ (\text{type II}), \end{cases} \tag{1}$$

relates a lattice vector in the parent, $\mathbf{a}_0$, to a vector in the twin, $\overline{\mathbf{a}}$, via $\overline{\mathbf{a}} = \overline{\mathbf{Q}}\mathbf{a}_0$, as shown on the right of Fig. 1(c). The unit normal to the habit plane is $\mathbf{m}_0$, and the direction of shear is $\mathbf{s}_0$. The second-order unit tensor is denoted by $\mathbf{1}$. For centrosymmetric crystals, reflection $-\overline{\mathbf{Q}}$ is often used instead of (1) to describe the orientation of the twin relative to the parent. In crystals lacking a center of symmetry, the two rotations listed in (1) are augmented by their negatives, i.e., two complementary reflection operations (Christian and Mahajan, 1995), with all four operations then crystallographically distinct.

3. Continuum theory: nonlinear elasticity, slip, and twinning

A constitutive framework for crystals undergoing large thermoelastic, plastic, and twinning deformations is developed. The framework conforms to many established principles of continuum mechanics and thermodynamics of single crystal behavior, as described in Teodosiu (1970), Teodosiu and Sidoroff (1976), Clayton (2005), though these prior works did not explicitly consider twinning or possible residual volume changes resulting from dislocations and twin boundaries or stacking faults.

3.1. Kinematics

A small volume element of crystalline material of fixed mass is assigned reference coordinates $\mathbf{X}$. Let $\mathbf{x} = \varphi(\mathbf{X}, t)$ denote spatial coordinates of the element, with φ the motion. Deformation gradient $\mathbf{F}$ for the element is

$$\mathbf{F} = \frac{\partial \mathbf{x}}{\partial \mathbf{X}}, \tag{2}$$

decomposed multiplicatively into a series of terms:

$$\mathbf{F} = \mathbf{F}^{\mathbf{E}} \overline{J}^{1/3} \mathbf{F}^{\mathbf{I}} \mathbf{F}^{\mathbf{P}} = \mathbf{F}^{\mathbf{E}} \overline{\mathbf{F}}^{\mathbf{I}} \mathbf{F}^{\mathbf{P}} = \mathbf{F}^{\mathbf{E}} \overline{\mathbf{F}} = \mathbf{F}^{\mathbf{L}} \widehat{\mathbf{F}}. \tag{3}$$

Here, $\mathbf{F}^{\mathbf{E}}$ accounts for recoverable thermoelastic deformation and rigid body rotation, $\overline{\mathbf{F}}^{\mathbf{I}} = \overline{J}^{1/3} \mathbf{F}^{\mathbf{I}}$ accounts for defect kinematics that alter the lattice, and $\mathbf{F}^{\mathbf{P}}$ accounts for lattice-preserving plastic slip. Twinning is modeled by term $\mathbf{F}^{\mathbf{I}}$, accounting for the average, irreversible shape deformation resulting from one or more twins that may nucleate and propagate in a volume element of fixed mass of crystal. Volume changes associated with defects are addressed by scalar $\overline{J}$. The total irreversible deformation is $\overline{\mathbf{F}} = \overline{\mathbf{F}}^{\mathbf{I}} \mathbf{F}^{\mathbf{P}}$. The total elastic lattice deformation (recoverable and residual) is $\mathbf{F}^{\mathbf{L}} = \mathbf{F}^{\mathbf{E}} \overline{J}^{1/3} \mathbf{1}$, and the remaining deformation from defect motion (dislocation glide and twinning) is $\widehat{\mathbf{F}} = \mathbf{F}^{\mathbf{I}} \mathbf{F}^{\mathbf{P}}$.

Denote by $\mathbf{g}(\mathbf{x})$ and $\mathbf{G}(\mathbf{X})$ metric tensors associated with possibly curvilinear coordinate systems in configurations B and B_0, with components $g_{ab} = \mathbf{g}_a \cdot \mathbf{g}_b$ and $G_{AB} = \mathbf{G}_A \cdot \mathbf{G}_B$ (Eringen, 1962). Basis vectors in spatial and referential coordinate systems are $\mathbf{g}_a$ and $\mathbf{G}_A$, respectively ($a, A = 1, 2, 3$). Let all intermediate configurations be referred to an external Cartesian coordinate system with metric tensor components $\delta_{\alpha\beta}(\alpha = 1, 2, 3)$. Let the Jacobian determinants of deformation mappings in (3) associated with volume changes be formally defined as

$$J = \sqrt{\frac{\det \mathbf{g}}{\det \mathbf{G}}} \det \mathbf{F} = J^E \overline{J} J^I J^P = J^L J^I J^P, \quad J^E = \sqrt{\det \mathbf{g}} \det \mathbf{F}^{\mathbf{E}}, \quad J^I = \det \mathbf{F}^{\mathbf{I}}, \quad J^P = \sqrt{\frac{1}{\det \mathbf{G}}} \det \mathbf{F}^{\mathbf{P}}. \tag{4}$$

As will be demonstrated explicitly later in (12), the isochoric character of slip and twinning leads to the conditions $J^I = J^P = 1$ (no volume changes associated with twinning or slip) and $J = J^E \overline{J} = J^L$ (volume changes associated only with recoverable and residual thermoelasticity). The residual elastic volume change $\overline{J}$ arising from distributed defects such as dislocation lines is derived from the assertion that in continuum nonlinear elasticity, the average strain of a body containing residual stress fields arising from internal displacement discontinuities need not vanish even if the traction on its external surfaces vanishes (Toupin and Rivlin, 1960; Teodosiu, 1982; Clayton and Bammann, 2009). Presently, only volume changes are considered, e.g., corresponding to random defect distributions imparting no preferred directions in average residual elastic strains, though more general treatments allowing for shape changes resulting from residual stresses associated with crystal defects at multiple length scales have been suggested (Clayton and McDowell, 2003; Clayton et al., 2004a, 2005, 2006; McDowell, 2008; Clayton and Bammann, 2009). In Section 4.4, relationships between $\overline{J}$, the line density of dislocations, and nonlinear thermoelastic properties are given, with explicit formulae for $\overline{J}$ listed in (65) and (66) following from previous studies (Zener, 1942; Seeger and Haasen, 1958; Toupin and Rivlin, 1960; Holder and Granato, 1969; Teodosiu, 1982; Clayton and Bammann, 2009). In the present context, $\mathbf{F}^{\mathbf{P}}$ and $\mathbf{F}^{\mathbf{I}}$ account for isochoric deformations resulting from respective motion of slip dislocations and twinning partials, while $\overline{J}$ accounts for volume changes resulting from the residual stress fields of the defects themselves.

Introduced next are sets of contravariant and covariant vectors denoting directions and planes, respectively, for slip and twinning. When referred to the reference lattice prior to any reorientation by twinning, these are denoted by $\{\mathbf{s}_0^i, \mathbf{m}_0^i\}$ for each slip system i, and $\{\mathbf{s}_0^j, \mathbf{m}_0^j\}$ for each twin system j. The total number of slip systems is n, and the total number of twin systems is w. Reference shearing directions and plane normals are all of unit length, and each pair of contravariant shear direction and covariant plane normal is orthogonal:

$$\mathbf{s}_0^i \cdot \mathbf{m}_0^i = 0, \quad |\mathbf{s}_0^i| = |\mathbf{m}_0^i| = 1 \ (\forall i = 1, \ldots n); \quad \mathbf{s}_0^j \cdot \mathbf{m}_0^j = 0, \quad |\mathbf{s}_0^j| = |\mathbf{m}_0^j| = 1 (\forall j = 1, \ldots w). \tag{5}$$

During the course of twinning, one or more parts (i.e., twins) of the volume element of crystal undergoes a rotation relative to the parent. In a volume fraction of the crystal undergoing twinning via mode j, slip directions and slip plane normals transform in the reference configuration according to the usual rules for contravariant and covariant vectors, that is

$$\mathbf{s}_{0j}^i = \overline{\mathbf{Q}}^j \mathbf{s}_0^i, \quad \mathbf{m}_{0j}^i = \mathbf{m}_0^i \overline{\mathbf{Q}}^{jT} \ (\forall i = 1, \ldots n \text{ slip systems}; \forall j = 1, \ldots w \text{ twin volumes}), \tag{6}$$

where $\overline{\mathbf{Q}}^j$ is the rotation found from (1) corresponding to particular twin system j. For example, if j is a type I twin, $\overline{\mathbf{Q}}^j = 2\mathbf{m}_0^j \otimes \mathbf{m}_0^j - \mathbf{1}$, while if j is a type II twin, $\overline{\mathbf{Q}}^j = 2\mathbf{s}_0^j \otimes \mathbf{s}_0^j - \mathbf{1}$. Notice from (6) that, within each twinned volume, updated slip directions $\mathbf{s}_{0j}^i$ and slip plane normals $\mathbf{m}_{0j}^i$ remain orthogonal and of unit length for each i. For simplicity, successive twinning is not considered. Hence, secondary twins that could form within already twinned regions, leading to reorientation of the twinning systems $\{\mathbf{s}_0^j, \mathbf{m}_0^j\}$, are not represented. Further reorientation of transformed directors in (6) is likewise prohibited once the twin is fully formed. Rotation (6) does not apply to the volume fraction of the grain comprising the parent. Plastic deformation $\mathbf{F}^P$ and twinning deformation $\mathbf{F}^I$ do not directly alter the directions associated with slip and twinning. The former is lattice-preserving, as discussed in Section 2.2, while the latter affects the lattice orientation indirectly via (6) and evolution of the twin volume fraction for each twin system j to be discussed later. However, thermoelastic deformation and residual elastic volume changes both affect the lattice directors:

$$\begin{aligned}
&\mathbf{s}^i = \mathbf{F}^L \mathbf{s}_0^i, \quad \mathbf{m}^i = \mathbf{m}_0^i \mathbf{F}^{L-1}, \quad \overline{\mathbf{s}}_0^i = \bar{J}^{1/3} \mathbf{s}_0^i, \quad \overline{\mathbf{m}}_0^i = \mathbf{m}_0^i \bar{J}^{-1/3} \ (\forall i = 1, \ldots n \in \text{ parent}), \\
&\mathbf{s}_j^i = \mathbf{F}^L \mathbf{s}_{0j}^i, \quad \mathbf{m}_j^i = \mathbf{m}_{0j}^i \mathbf{F}^{L-1}, \quad \overline{\mathbf{s}}_{0j}^i = \bar{J}^{1/3} \mathbf{s}_{0j}^i, \quad \overline{\mathbf{m}}_{0j}^i = \mathbf{m}_{0j}^i \bar{J}^{-1/3} \ (\forall i = 1, \ldots n \in \text{ twins } j = 1, \ldots w), \\
&\mathbf{s}^j = \mathbf{F}^L \mathbf{s}_0^j, \quad \mathbf{m}^j = \mathbf{m}_0^j \mathbf{F}^{L-1}, \quad \overline{\mathbf{s}}_0^j = \bar{J}^{1/3} \mathbf{s}_0^j, \quad \overline{\mathbf{m}}_0^j = \mathbf{m}_0^j \bar{J}^{-1/3} \ (\forall j = 1, \ldots w \in \text{ parent}).
\end{aligned} \tag{7}$$

The effect of $\bar{J}$ on the slip directors and slip plane normals was omitted in earlier work (Clayton, 2009).

An additional remark on notation is in order. Subscripts and superscripts following mathematical objects in bold font correspond to slip or twin systems (e.g., i or j), and are not subject to usual conventions associated with the index notation such as Einstein's summation convention. Furthermore, such subscripts and superscripts do not require placeholder periods frequently used for components of mixed contra-covariant tensors (Schouten, 1954). For example, the deformation gradient is often written in geometric settings as $\mathbf{F} = F_{.A}^a \mathbf{g}_a \otimes \mathbf{G}^A$ (Clayton et al., 2005), while slip direction vector for system i within twin system j is written here as $\mathbf{s}_j^i = s_j^{ia} \mathbf{g}_a$ and not as $\mathbf{s}_{.j}^i$, since i and j do not refer to components of a vector or tensor in this case.

Fig. 2 depicts the physics underlying (2)–(7) for a crystal with a single slip system and a single twin. Multiplicative decomposition (3) implies a series of configurations of the material element. The reference configuration is labeled B_0 with
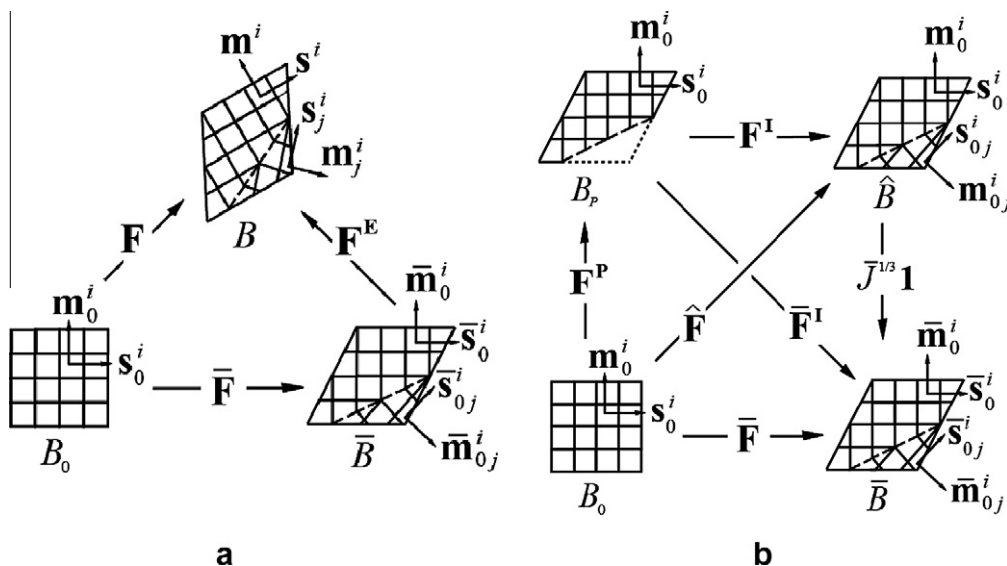

Fig. 2. Deformations and slip system geometry for crystal deforming by elasticity, slip, and twinning: (a) total deformation and (b) residual deformation.

corresponding coordinates $\mathbf{X}$, the spatial configuration is labeled B with corresponding coordinates $\mathbf{x}$, and the elastically un-loaded intermediate configuration is labeled $\overline{B}$. Since $\mathbf{F}^{E-1}$ and $\overline{\mathbf{F}}$ are in general not integrable, continuous coordinates spanning $\overline{B}$ do not exist (Clayton et al., 2004b, 2005). However, elastic and inelastic deformations act as tangent maps (Marsden and Hughes, 1983) between configurations via $\mathbf{F}^E : T\overline{B} \rightarrow TB$ and $\overline{\mathbf{F}} : TB_0 \rightarrow T\overline{B}$. Additional configurations B_P and $\widehat{B}$ are implied by the inelastic tangent maps $\mathbf{F}^P : TB_0 \rightarrow TB_P, \mathbf{F}^I : TB_P \rightarrow T\widehat{B}$, and $\overline{J}^{1/3}\mathbf{1} : T\widehat{B} \rightarrow T\overline{B}$. The total deformation gradient is illustrated in Fig. 2(a). In Fig. 2(b), individual maps comprising the residual deformation $\overline{\mathbf{F}} = \mathbf{F}^{E-1}\mathbf{F} = \overline{J}^{1/3}\mathbf{F}^I\mathbf{F}^P$ are shown. For clarity, the implicit effect of twinning on the orientation of the plastically slipped lattice in configuration B_P is not shown; i.e., only the parent is shown in the illustration of configuration B_P.

The spatial velocity gradient following from (2) and (3) is

$$\mathbf{L} = \dot{\mathbf{F}}\mathbf{F}^{-1} = \dot{\mathbf{F}}^E\mathbf{F}^{E-1} + \mathbf{F}^E\dot{\mathbf{F}}^I\mathbf{F}^{I-1}\mathbf{F}^{E-1} + \mathbf{F}^E\mathbf{F}^I\dot{\mathbf{F}}^P\mathbf{F}^{P-1}\mathbf{F}^{I-1}\mathbf{F}^{E-1} + (1/3)\dot{\overline{J}}\overline{J}^{-1}\mathbf{1}. \tag{8}$$

The inelastic velocity gradient referred to configuration $\overline{B}$ is

$$\dot{\overline{\mathbf{F}}}\overline{\mathbf{F}}^{-1} = \dot{\mathbf{F}}^I\mathbf{F}^{I-1} + \mathbf{F}^I\dot{\mathbf{F}}^P\mathbf{F}^{P-1}\mathbf{F}^{I-1} + (1/3)\dot{\overline{J}}\overline{J}^{-1}\mathbf{1} = \mathbf{L}^I + \overline{\mathbf{L}}^P + (1/3)\dot{\overline{J}}\overline{J}^{-1}\mathbf{1}, \tag{9}$$

where

$$\mathbf{L}^I = \dot{\mathbf{F}}^I\mathbf{F}^{I-1} = \underbrace{\sum_{j=1}^{w}\dot{f}^j\gamma^j\overline{\mathbf{s}}_0^j \otimes \overline{\mathbf{m}}_0^j}_{\text{twinning in parent crystal}} \tag{10}$$

results from twinning shears, and

$$\overline{\mathbf{L}}^P = \mathbf{F}^I\underbrace{\dot{\mathbf{F}}^P\mathbf{F}^{P-1}}_{\mathbf{L}^P}\mathbf{F}^{I-1} = \underbrace{(1-f_T)\sum_{i=1}^{n}\dot{\gamma}^i\overline{\mathbf{s}}_0^i \otimes \overline{\mathbf{m}}_0^i}_{\text{slip in parent crystal}} + \underbrace{\sum_{j=1}^{w}\left(f^j\sum_{i=1}^{n}\dot{\gamma}_j^i\overline{\mathbf{s}}_{0j}^i \otimes \overline{\mathbf{m}}_{0j}^i\right)}_{\text{slip in twinned crystal}} \tag{11}$$

results from slip in parent and twinned domains. In (10), γ^j is the predefined shear associated with twin system j, a positive scalar that is fixed for all twins in a given family of twin systems. In (11), $\dot{\gamma}^i$ is the slip rate on system i in the parent grain, and $\dot{\gamma}_j^i$ is the slip rate on system i within reoriented twin fraction j. The volume fraction of crystal occupied by twin j, measured per unit volume in configuration $\overline{B}$, is labeled by the scalar $f^j \geqslant 0$, with time rate $\dot{f}^j$ (Chin et al., 1969; Van Houtte, 1978). The total volume fraction of twinned crystal is $f_T = \sum f^j$, subject to the restriction $0 \leqslant f_T \leqslant 1$. Detwinning is not considered; hence, $\dot{f}^j \geqslant 0$. In the interior summation within the rightmost term of (11), the slip directors and slip plane normals in the twinned regions are found according to (6), where the particular form of $\overline{\mathbf{Q}}^j$ corresponds to the twin with associated value of f^j in the outer summation.

Since for each slip or twin system, the shear directions and plane normals are orthogonal,

$$\mathrm{tr}\mathbf{L}^I = \mathrm{tr}\overline{\mathbf{L}}^P = 0 \Rightarrow \dot{J}^I = \dot{J}^P = 0 \Rightarrow J^I = J^P = 1 \quad (t \geqslant 0), \tag{12}$$

since at $t = 0, \mathbf{F}^I$ and $\mathbf{F}^P$ both reduce to the unit tensor in corresponding coordinate systems leading to $J^I(t=0) = J^P(t=0) = 1$, and where $\mathrm{tr}\mathbf{A} = A_a^a$ for a second-order matrix $\mathbf{A}$. A formal derivation of (12) is given in Appendix A. Thus, (9)–(11) properly reflect the isochoric nature of slip and twinning, and together with (3) and (4), require that all volume changes be accommodated thermoelastically via J^E and/or by defect generation via $\overline{J}$, such that the first of (4) reduces to $J = J^E\overline{J} = J^L$.

When $\overline{J} = 1$ and $\dot{f}^j = 0$ for all j, $\mathbf{F}^I = \mathbf{1}, \overline{\mathbf{F}} = \mathbf{F}^P$, and $\mathbf{L}^P$ in (11) reduces to its usual definition from crystal plasticity theory (Teodosiu and Sidoroff, 1976; Asaro, 1983; Clayton, 2005). In this simplified case, all inelastic deformation occurs via slip, $\overline{\mathbf{F}}$ is lattice-preserving, and the lattice directors remain unchanged between configurations B_0 and $\overline{B}$. On the other hand, when twinning does takes place, $\mathbf{F}^I$ does not act as a true elastic lattice deformation in the sense of (7) and Born and Huang (1954), since only that part of the lattice within the twinned volume undergoes a transformation, and this transformation occurs via rotation (6) and does not include any stretch of the lattice directors.

Remarks on the order of terms in multiplicative decomposition (3) are now merited. The recoverable thermoelastic deformation $\mathbf{F}^E$ is logically placed first in the decomposition, following the usual scheme of crystal plasticity theory (Teodosiu and Sidoroff, 1976; Asaro, 1983), so that thermoelastic unloading proceeds via pre-multiplication of $\mathbf{F}$ by $\mathbf{F}^{E-1}$ and so that the lattice director vectors are mapped to the current configuration via (7). The remaining three terms in the decomposition are placed in order of decreasing effect on the crystal lattice (i.e., on the lattice director vectors). Term $\overline{J}^{1/3}\mathbf{1}$ is placed second in the decomposition because it affects the volume of the crystal and imparts a stretch to the lattice directors as indicated in (7); however, its precise placement is of apparently lesser mathematical importance because this term is spherical (i.e., isotropic). Term $\mathbf{F}^I$ is placed next because twinning affects the lattice director vectors implicitly, via the rotation or reflection operation in (6). Term $\mathbf{F}^P$ is placed last in the decomposition because plastic slip does not directly affect the lattice directors (Asaro, 1983). Placement of $\mathbf{F}^I$ before $\mathbf{F}^P$ in (3) does not imply that during the time history of a given deformation process, twinning always takes place before slip, or vice-versa. All elastic and inelastic deformation modes in (3) can occur simultaneously in time. This argument applies similarly in the context of traditional crystal plasticity (i.e., no twinning) wherein $\mathbf{F} = \mathbf{F}^E\mathbf{F}^P$ holds: for example, elastic deformation and plastic deformation can both occur simultaneously at a given time

as an increasing load is applied to a strain hardening crystal. An alternative decomposition in which $\mathbf{F^I}$ and $\mathbf{F^P}$ are interchanged in (3) is explored in Appendix B.

Defect content associated with incompatibility of the total lattice deformation $\mathbf{F^L}$ (Teodosiu, 1970; Regueiro et al., 2002; Clayton et al., 2004a,b, 2005) is measured by two-point geometrically necessary dislocation tensor $\boldsymbol{\alpha_G}$ satisfying

$$B^\alpha = -\int_c F^{L-1\alpha}_{\cdot a} dx^a = -\int_C \widehat{F}^\alpha_{\cdot A} dX^A = \int_A \alpha^{\alpha A}_G N_A dA, \quad \alpha^{\alpha A}_G = \varepsilon^{ABC} \widehat{F}^\alpha_{\cdot B,C} = \varepsilon^{ABC} \widehat{F}^\alpha_{\cdot [B,C]}, \tag{13}$$

where B^α are components (indices referred to configuration $\widehat{B}$) of a total Burgers vector associated with circuit c in the spatial configuration or circuit C in the reference configuration, A is the area enclosed by C with unit normal components N_A, and ε^{ABC} are contravariant components of the permutation tensor. Stokes's theorem is used to convert from the line integral to the area integral in the third equality of (13). From (3),

$$\alpha^{\alpha A}_G = \varepsilon^{ABC} \widehat{F}^\alpha_{\cdot [B,C]} = \underbrace{\varepsilon^{ABC} F^{I\alpha}_{\cdot \beta} F^{P\beta}_{\cdot B,C}}_{\text{slip gradients}} + \underbrace{\varepsilon^{ABC} F^{I\alpha}_{\cdot \beta,C} F^{P\beta}_{\cdot B}}_{\text{twin gradients}}. \tag{14}$$

Contributions of plastic slip gradients to the geometrically necessary dislocation density tensor corresponding to the first term following the second equality in (14) are well-documented in papers dealing with the continuum theory of dislocations (Ashby, 1970; Teodosiu, 1970; Fleck et al., 1994; Arsenlis and Parks, 1999; Voyiadjis and Abu Al-Rub, 2007; Rezvanian et al., 2007; Clayton et al., 2008). The second term in the sum on the right arises from material gradients of twinning shear, for example gradients of twin volume fractions arising during propagation of tapered twins (Scott and Orr, 1983); the contribution to the dislocation density tensor in this case would be partial dislocations at interfaces between twin and parent or between intersecting twins. Applying Nanson's formula to (13), the geometrically necessary dislocation tensor in intermediate configuration $\widehat{B}$ of Fig. 2(b), labeled $\hat{\boldsymbol{\alpha}}$, is

$$\hat{\alpha}^{\alpha\beta} = \widehat{J}^{-1} \widehat{F}^\beta_{\cdot A} \alpha^{\alpha A}_G = J^L F^{L-1\beta}_{\cdot a} \varepsilon^{abc} F^{L\alpha}_{\cdot [b,c]} = \sum_i \rho^i b^\alpha \varsigma^\beta, \tag{15}$$

where $\widehat{J} = J^I J^P = 1$ by (12), and the second equality in (15) reduces to Nye's relation (Nye, 1953) between the dislocation density tensor and the lattice curvature in the limit of small elastic deformations. The sum on the far right of (15) is invoked over dislocation populations of index label i, where ρ^i is the length per unit volume of dislocation segments with unit tangent line vector ς^β and Burgers vector b^α. Nye's original treatment (Nye, 1953) was in part based on observations of slip traces in transparent corundum, and hence is of particular relevance in the present application to ceramics and corundum in particular. In (13)–(15), sufficient differentiability of $\mathbf{F^E}, \mathbf{F^I}, \mathbf{F^P}$, and $\widehat{J}$ has been assumed. Discontinuities in the deformation gradient or in the Bravais lattice, for example singularities across slipped regions or at dislocation cores (Teodosiu, 1970, 1982) and jumps in deformation gradient across twin boundaries (James, 1981; Bhattacharya, 1991) are not resolved explicitly in the present continuum framework that addresses defects via continuous distributions (Willis, 1967).

Non-dimensional internal state variables are introduced to represent energetic changes associated with two other kinds of defects. The first such internal state variable is a measure of the density of statistically stored dislocations (Ashby, 1970; Arsenlis and Parks, 1999; Bammann, 2001; Clayton et al., 2004a, 2006) that accumulate with homogeneous slip, $\xi = b\sqrt{\rho_S}$, where b is a scalar Burgers vector—or a constant on the order of a lattice parameter when the crystal exhibits slip on systems with different Burgers vectors—and ρ_S is the total length of such dislocations per unit volume in $\overline{B}$. Statistically stored dislocations include closed loops and dipoles that do not contribute to the total Burgers vector B^α in (13). The second internal state variable measures the total density of twin boundaries, $\zeta = \sqrt{b\eta_T}$, where η_T is the total area of twin boundaries measured per unit volume in configuration $\overline{B}$.

3.2. Constitutive assumptions

Let ρ and ρ_0 denote mass density of the solid in current and reference configurations, respectively, related by $\rho_0 = \rho J$. Let $\overline{\rho} = \rho J^E = \rho_0 \overline{J}^{-1}$ denote mass density in configuration $\overline{B}$. The forthcoming thermodynamic analysis is conducted in $\overline{B}$, the natural configuration that serves as an evolving reference configuration for the instantaneous thermoelastic response of the crystal (Eckart, 1948; Scheidler and Wright, 2001; Clayton et al., 2004a, 2006; Clayton, 2005). The Helmholtz free energy per unit volume in $\overline{B}$ is $\overline{\Psi} = \overline{\rho}\psi$, with ψ the free energy per unit mass. The free energy exhibits the dependencies

$$\overline{\Psi} = \overline{\Psi}\left(\mathbf{E^E}, \theta, \hat{\boldsymbol{\alpha}}, \xi, \zeta, \{f^j\}\right), \tag{16}$$

where θ is the absolute temperature. Electric polarization (e.g., of sapphire) is not addressed in (16) since the present study is limited to situations where electric fields are absent. Variables $\hat{\boldsymbol{\alpha}}, \xi$, and ζ are, respectively, related to densities of geometrically necessary dislocations, statistically stored dislocations, and twin boundaries, as discussed in Section 3.1. Set $\{f^j\}$ includes each of the twin volume fractions, and

$$E^E_{\alpha\beta} = \frac{1}{2}\left(C^E_{\alpha\beta} - \delta_{\alpha\beta}\right) = \frac{1}{2}\left(F^{Ea}_{\cdot\alpha} g_{ab} F^{Eb}_{\cdot\beta} - \delta_{\alpha\beta}\right) \tag{17}$$

is a finite elastic strain tensor associated with elastic deformation tensor $\mathbf{C}^{\mathbf{E}}$, with components referred to an assumed extrinsic Cartesian frame on $\overline{B}$ with basis vectors not tangent to possibly anholonomic intermediate material lines (Clayton et al., 2004b, 2005). In agreement with physical arguments of Sections 2.2 and 2.3, the free energy does not depend explicitly on plastic deformation or twinning shears.

3.3. Thermodynamics

The standard local forms of the balance of energy and dissipation inequality, respectively, each referred to the reference configuration, are (Eringen, 1962; Marsden and Hughes, 1983)

$$\rho_0 \dot{e} = \mathbf{\Sigma} : \dot{\mathbf{E}} - \nabla_0 \cdot \mathbf{Q} + \rho_0 r, \quad \mathbf{\Sigma} : \dot{\mathbf{E}} - \rho_0 \left(\dot{\psi} + \eta \dot{\theta} \right) - \frac{1}{\theta} \nabla_0 \theta \cdot \mathbf{Q} \geqslant 0. \tag{18}$$

In (18), $e = \psi + \theta \eta$ is internal energy per unit mass, with η the entropy per unit mass. Symmetric second Piola–Kirchhoff stress $\mathbf{\Sigma}$ is related to first Piola–Kirchhoff stress $\mathbf{P}$ and symmetric Cauchy stress $\boldsymbol{\sigma}$ by

$$\Sigma^{AB} = F_{\cdot a}^{-1A} P^{aB} = J F_{\cdot a}^{-1A} \sigma^{ab} F_{\cdot b}^{-1B}. \tag{19}$$

Symmetric tensor $\mathbf{E} = (1/2)(\mathbf{F}^T \mathbf{F} - \mathbf{G})$ is the right Cauchy–Green strain, ∇_0 is the covariant derivative on B_0, $\mathbf{Q}$ is the heat flux, and scalar r denotes other heat sources of energy per unit mass, e.g., radiation. Stress power per unit intermediate volume can be written

$$\bar{J}^{-1} \Sigma^{AB} \dot{E}_{AB} = \left(J^E F_{\cdot b}^{E-1\beta} \sigma_a^{\cdot b} F_{\cdot \alpha}^{Ea} \right) \left(F_{\cdot e}^{E-1\alpha} L_{\cdot d}^e F_{\cdot \beta}^{Ed} \right) = \overline{M}_\alpha^{\cdot \beta} \overline{L}_{\cdot \beta}^\alpha, \tag{20}$$

where Mandel's stress (Mandel, 1974) is $\overline{\mathbf{M}} = \mathbf{C}^{\mathbf{E}} \overline{\mathbf{\Sigma}}$, the symmetric elastic second Piola–Kirchhoff stress is $\overline{\mathbf{\Sigma}} = J^E \mathbf{F}^{\mathbf{E}-1} \boldsymbol{\sigma} \mathbf{F}^{\mathbf{E}-T}$, and the velocity gradient pulled back to $\overline{B}$ is

$$\overline{\mathbf{L}} = \mathbf{F}^{\mathbf{E}-1} \mathbf{L} \mathbf{F}^{\mathbf{E}} = \mathbf{F}^{\mathbf{E}-1} \dot{\mathbf{F}}^{\mathbf{E}} + \mathbf{L}^{\mathbf{I}} + \overline{\mathbf{L}}^{\mathbf{P}} + (1/3) \dot{\overline{J}} \overline{J}^{-1} \mathbf{1}. \tag{21}$$

The time rate of free energy change per unit intermediate configuration volume is

$$\dot{\overline{\Psi}} = \frac{d}{dt} (\overline{\rho} \psi) = \bar{J}^{-1} \rho_0 \left(\dot{\psi} - \dot{\overline{F}}_{\cdot A}^\alpha \overline{F}_{\cdot \alpha}^{-1A} \psi \right) = \overline{\rho} \dot{\psi} - \overline{\Psi} \dot{\overline{J}} \overline{J}^{-1}, \tag{22}$$

and following from (21) and the symmetry of $\overline{\mathbf{\Sigma}}$ and $\dot{\mathbf{E}}^{\mathbf{E}}$,

$$\overline{M}_\alpha^{\cdot \beta} \overline{L}_{\cdot \beta}^\alpha = \overline{\Sigma}^{\beta \delta} \dot{E}_{\delta \beta}^E + \overline{M}_\alpha^{\cdot \beta} L_{\cdot \beta}^{I\alpha} + \overline{M}_\alpha^{\cdot \beta} \overline{L}_{\cdot \beta}^{P\alpha} + (1/3) \dot{\overline{J}} \overline{J}^{-1} \overline{M}_\beta^{\cdot \beta}. \tag{23}$$

Expanding the rate of $\overline{\Psi}$ of (16) using the chain rule (Coleman and Gurtin, 1967),

$$\dot{\overline{\Psi}} = \frac{\partial \overline{\Psi}}{\partial \mathbf{E}^{\mathbf{E}}} : \dot{\mathbf{E}}^{\mathbf{E}} + \frac{\partial \overline{\Psi}}{\partial \theta} \dot{\theta} + \frac{\partial \overline{\Psi}}{\partial \hat{\boldsymbol{\alpha}}} : \dot{\hat{\boldsymbol{\alpha}}} + \frac{\partial \overline{\Psi}}{\partial \xi} \dot{\xi} + \frac{\partial \overline{\Psi}}{\partial \zeta} \dot{\zeta} + \frac{\partial \overline{\Psi}}{\partial f^j} \dot{f}^j, \tag{24}$$

with summation implied over w twin fractions j, the entropy inequality in (18) can be written

$$\left(\overline{\mathbf{\Sigma}} - \frac{\partial \overline{\Psi}}{\partial \mathbf{E}^{\mathbf{E}}} \right) : \dot{\mathbf{E}}^{\mathbf{E}} - \left(\overline{N} + \frac{\partial \overline{\Psi}}{\partial \theta} \right) \dot{\theta} + \overline{\mathbf{\Pi}} : \left(\mathbf{L}^{\mathbf{I}} + \overline{\mathbf{L}}^{\mathbf{P}} + \frac{\dot{\overline{J}}}{3\overline{J}} \mathbf{1} \right) \geqslant \frac{\partial \overline{\Psi}}{\partial \hat{\boldsymbol{\alpha}}} : \dot{\hat{\boldsymbol{\alpha}}} + \frac{\partial \overline{\Psi}}{\partial \xi} \dot{\xi} + \frac{\partial \overline{\Psi}}{\partial \zeta} \dot{\zeta} + \frac{\partial \overline{\Psi}}{\partial f^j} \dot{f}^j + \frac{1}{\theta} \overline{\nabla} \theta \cdot \overline{\mathbf{q}}, \tag{25}$$

where $\overline{N} = \overline{\rho} \eta$ is the entropy per unit intermediate volume, $\overline{\nabla} \theta = \nabla_0 \theta \overline{\mathbf{F}}^{-1}$ is the intermediate temperature gradient, $\overline{\mathbf{q}} = \bar{J}^{-1} \overline{\mathbf{F}} \mathbf{Q}$ is the intermediate heat flux, and

$$\overline{\mathbf{\Pi}} = \overline{\mathbf{M}} - \overline{\Psi} \mathbf{1} \tag{26}$$

is a (negative) version of Eshelby's energy-momentum tensor or Eshelby's stress tensor (Eshelby, 1975; Maugin, 1994; Clayton et al., 2004a, 2006) mapped to configuration $\overline{B}$. Following standard arguments (Coleman and Gurtin, 1967; Scheidler and Wright, 2001; Clayton, 2005), stress–elastic strain and entropy-temperature relations are deduced:

$$\overline{\mathbf{\Sigma}} = \frac{\partial \overline{\Psi}}{\partial \mathbf{E}^{\mathbf{E}}}, \quad \overline{N} = -\frac{\partial \overline{\Psi}}{\partial \theta}, \quad \boldsymbol{\sigma} = J^{E-1} \mathbf{F}^{\mathbf{E}} \frac{\partial \overline{\Psi}}{\partial \mathbf{E}^{\mathbf{E}}} \mathbf{F}^{\mathbf{E}T}, \quad \eta = -\overline{\rho}^{-1} \frac{\partial \overline{\Psi}}{\partial \theta}. \tag{27}$$

The rightmost term of (25) contributes positively to dissipation upon prescription of the conduction law

$$\overline{\mathbf{q}} = -\overline{\mathbf{K}} \overline{\nabla} \theta, \quad -\overline{\nabla} \theta \cdot \overline{\mathbf{q}} = \overline{\nabla} \theta \cdot \overline{\mathbf{K}} \overline{\nabla} \theta \geqslant 0, \tag{28}$$

where $\overline{\mathbf{K}}$ is a symmetric and positive definite matrix of thermal conductivity. Applying (27) and (28),

$$\overline{\mathbf{\Pi}} : \mathbf{L}^{\mathbf{I}} + \overline{\mathbf{\Pi}} : \overline{\mathbf{L}}^{\mathbf{P}} + \frac{\dot{\overline{J}}}{3\overline{J}} \text{tr} \overline{\mathbf{\Pi}} \geqslant \frac{\partial \overline{\Psi}}{\partial \hat{\boldsymbol{\alpha}}} \dot{\hat{\boldsymbol{\alpha}}} + \frac{\partial \overline{\Psi}}{\partial \xi} \dot{\xi} + \frac{\partial \overline{\Psi}}{\partial \zeta} \dot{\zeta} + \frac{\partial \overline{\Psi}}{\partial f^j} \dot{f}^j - \frac{1}{\theta} \overline{\nabla} \theta \cdot \overline{\mathbf{K}} \overline{\nabla} \theta \tag{29}$$

is the reduced dissipation inequality. In the absence of temperature gradients, (29) requires that the energy dissipated by twinning, slip, and residual volume changes exceeds the rate of energy storage associated with defects, specifically geometrically necessary and statistically stored dislocations and twin boundaries. From (9)–(11), energies dissipated from twinning and slip, respectively, can be written

$$\overline{\mathbf{\Pi}}:\mathbf{L}^{\mathbf{I}}=\sum_{j=1}^{w}\overline{\tau}^j\dot{f}^j\gamma^j,\quad\overline{\mathbf{\Pi}}:\overline{\mathbf{L}}^{\mathbf{P}}=(1-f_T)\sum_{i=1}^{n}\overline{\tau}^i\dot{\gamma}^i+\sum_{j=1}^{w}\left(f^j\sum_{i=1}^{n}\overline{\tau}_j^i\dot{\gamma}_j^i\right),\tag{30}$$

where the driving forces are resolved stresses on each twin or slip plane, acting in the direction of shear:

$$\overline{\tau}^j=\overline{s}_0^{j\alpha}\overline{\Pi}_\alpha^{.\beta}\overline{m}_{0\beta}^j=J^E s^{ja}\sigma_a^{.b}m_b^j,\quad\overline{\tau}^i=\overline{s}_0^{i\alpha}\overline{\Pi}_\alpha^{.\beta}\overline{m}_{0\beta}^i=J^E s^{ia}\sigma_a^{.b}m_b^i,\quad\overline{\tau}_j^i=\overline{s}_{0j}^{i\alpha}\overline{\Pi}_\alpha^{.\beta}\overline{m}_{0j\beta}^i=J^E s_j^{ia}\sigma_a^{.b}m_{jb}^i.\tag{31}$$

Specific heat at constant elastic strain, measured per unit volume in configuration $\overline{B}$, is introduced as

$$\overline{c}=\frac{\partial\overline{E}}{\partial\theta}=-\theta\frac{\partial^2\overline{\Psi}}{\partial\theta^2},\tag{32}$$

where $\overline{E}=\overline{\rho}e$ is internal energy per intermediate volume. Multiplying the first of (18) by $\overline{J}^{-1}$, and using (19)–(24), (26)–(28), (32), the energy balance can be written in the intermediate configuration as

$$\underbrace{\overline{c}\dot{\theta}}_{\text{temperature change}}=\underbrace{\overline{\mathbf{\Pi}}:\left(\mathbf{L}^{\mathbf{I}}+\overline{\mathbf{L}}^{\mathbf{P}}\right)}_{\text{dissipation from slip and twinning}}+\underbrace{\left(\text{tr}\overline{\mathbf{\Pi}}+3\theta\frac{\partial\overline{\Psi}}{\partial\theta}\right)\frac{\dot{\overline{J}}}{3\overline{J}}}_{\text{dissipation from defect generation}}-\underbrace{\theta\overline{\beta}:\dot{\mathbf{E}}^{\mathbf{E}}}_{\text{thermoelastic coupling}}+\underbrace{\breve{\nabla}\cdot\overline{\mathbf{K}}\nabla\theta}_{\text{heat conduction}}$$

$$-\underbrace{\left(\frac{\partial\overline{\Psi}}{\partial\hat{\boldsymbol{\alpha}}}-\theta\frac{\partial^2\overline{\Psi}}{\partial\theta\partial\hat{\boldsymbol{\alpha}}}\right):\dot{\hat{\boldsymbol{\alpha}}}}_{\text{strain energy of geometrically necessary dislocations}}-\underbrace{\left(\frac{\partial\overline{\Psi}}{\partial\xi}-\theta\frac{\partial^2\overline{\Psi}}{\partial\theta\partial\xi}\right)\dot{\xi}}_{\text{strain energy of statistically stored dislocations}}-\underbrace{\left(\frac{\partial\overline{\Psi}}{\partial\zeta}-\theta\frac{\partial^2\overline{\Psi}}{\partial\theta\partial\zeta}\right)\dot{\zeta}}_{\text{surface energy of twin boundaries}}-\underbrace{\left(\frac{\partial\overline{\Psi}}{\partial f^j}-\theta\frac{\partial^2\overline{\Psi}}{\partial\theta\partial f^j}\right)\dot{f}^j}_{\text{energy of lattice reorientation from twinning}},\tag{33}$$

where source r of (18) is assumed absent in (33) and hereafter. Thermal stress coefficients in (33) are

$$\overline{\boldsymbol{\beta}}=-\frac{\partial^2\overline{\Psi}}{\partial\theta\partial\mathbf{E}^{\mathbf{E}}},\tag{34}$$

and the anholonomic covariant derivative in (33) is $\breve{\nabla}_\alpha=\overline{\nabla}_\alpha+\overline{J}^{-1}\overline{F}_{.A}^\beta\overline{\nabla}_\beta(\overline{J}F_{.\alpha}^{-1A})$ with $\overline{\nabla}_\alpha=\nabla_{0A}\overline{F}_{.\alpha}^{-1A}$. Note $\breve{\nabla}_\alpha=\overline{\nabla}_\alpha$ only when compatibility condition $\overline{F}_{.[A,B]}^\alpha=0$ holds and $\nabla_{0A}(\partial\overline{J}/\partial\overline{F}_{.A}^\alpha)=\nabla_{0A}(\overline{J}F_{.\alpha}^{-1A})=0$.

3.4. Representative free energy potential

A particular form of (16) is posited for anisotropic crystals that may undergo large elastic deformations, temperature changes, twinning, and dislocation accumulation. The free energy is decomposed as

$$\overline{\Psi}=\overline{\Psi}^E\left(\mathbf{E}^{\mathbf{E}},\theta,\{f^j\}\right)+\overline{Y}(\theta)+\overline{\Psi}^R(\hat{\boldsymbol{\alpha}},\xi,\zeta,\theta),\tag{35}$$

where $\overline{\Psi}^E$ accounts for the thermoelastic response, $\overline{Y}$ accounts for the specific heat content, and $\overline{\Psi}^R$ accounts for residual free energy of lattice defects. The thermoelastic energy consists of three terms:

$$\overline{\Psi}^E=\frac{1}{2}E_{\alpha\beta}^E{}^4\overline{\mathbb{C}}^{\alpha\beta\chi\delta}E_{\chi\delta}^E+\frac{1}{6}E_{\alpha\beta}^E{}^6\overline{\mathbb{C}}^{\alpha\beta\chi\delta\varepsilon\phi}E_{\chi\delta}^E E_{\varepsilon\phi}^E-\overline{\beta}^{\alpha\beta}E_{\alpha\beta}^E(\theta-\theta_0),\tag{36}$$

with the first term in (36) accounting for materially linear, but geometrically nonlinear, mechanical effects, the second accounting for materially nonlinear elastic effects important at high pressures (Graham and Brooks, 1971; Thurston, 1974), and the third accounting for thermoelastic coupling. Here, θ_0 is a constant temperature at which the lattice parameters exhibit their reference lengths, and remaining coefficients in (36) are partial derivatives of free energy at null elastic strain:

$$^4\overline{\mathbb{C}}^{\alpha\beta\chi\delta}=\frac{\partial^2\overline{\Psi}^E}{\partial E_{\alpha\beta}^E\partial E_{\chi\delta}^E}\bigg|_{\mathbf{E}^{\mathbf{E}}=\mathbf{0}},\quad{}^6\overline{\mathbb{C}}^{\alpha\beta\chi\delta\varepsilon\phi}=\frac{\partial^3\overline{\Psi}^E}{\partial E_{\alpha\beta}^E\partial E_{\chi\delta}^E\partial E_{\varepsilon\phi}^E}\bigg|_{\mathbf{E}^{\mathbf{E}}=\mathbf{0}},\quad\overline{\beta}^{\alpha\beta}=-\frac{\partial^2\overline{\Psi}^E}{\partial\theta\partial E_{\alpha\beta}^E}\bigg|_{\mathbf{E}^{\mathbf{E}}=\mathbf{0}}.\tag{37}$$

Coefficients in (37) may depend on temperature; when measured at a particular temperature, these are referred to as isothermal elastic constants. Superscripts 4 and 6 denote fourth- and sixth rank tensors of elastic coefficients, usually referred to (at fixed temperature) as second- and third-order isothermal elastic constants, respectively (Brugger, 1964; Thurston, 1974). Typically, small differences between isothermal elastic coefficients and their isentropic counterparts measured in sound speed experiments emerge from thermal expansion (Thurston, 1974).

In anisotropic solids, coefficients (37) depend on the orientation of the Bravais lattice in configuration $\overline{B}$. When twinning takes place, orientations of the original reference lattice (parent) and each twin differ. Here, a straightforward averaging method is used to define the effective coefficients for a volume element consisting of the parent and one or more twins.

It is assumed that elastic deformation $\mathbf{F}^E$ and elastic strain $\mathbf{E}^E$ act uniformly over the parent and twins comprising this volume element. Energy (36) is thus partitioned into contributions from the parent and each twin:

$$\overline{\Psi}^E = \frac{1}{2} E_{\alpha\beta}^E \, {}^4\overline{\mathbb{C}}_0^{\alpha\beta\chi\delta} E_{\chi\delta}^E (1-f_T) + \frac{1}{6} E_{\alpha\beta}^E \, {}^6\overline{\mathbb{C}}_0^{\alpha\beta\chi\delta\varepsilon\phi} E_{\chi\delta}^E E_{\varepsilon\phi}^E (1-f_T) - \overline{\beta}_0^{\alpha\beta} E_{\alpha\beta}^E (\theta - \theta_0)(1-f_T)$$
$$+ \sum_{j=1}^{w} \left[\frac{1}{2} E_{\alpha\beta}^E \, {}^4\overline{\mathbb{C}}_j^{\alpha\beta\chi\delta} E_{\chi\delta}^E + \frac{1}{6} E_{\alpha\beta}^E \, {}^6\overline{\mathbb{C}}_j^{\alpha\beta\chi\delta\varepsilon\phi} E_{\chi\delta}^E E_{\varepsilon\phi}^E - \overline{\beta}_j^{\alpha\beta} E_{\alpha\beta}^E (\theta - \theta_0) \right] f^j, \tag{38}$$

where ${}^4\overline{\mathbb{C}}_0^{\alpha\beta\chi\delta}, {}^6\overline{\mathbb{C}}_0^{\alpha\beta\chi\delta\varepsilon\phi}$, and $\overline{\beta}_0^{\alpha\beta}$ refer to coefficients for the parent lattice, and where for each twin j,

$$ {}^4\overline{\mathbb{C}}_j^{\alpha\beta\chi\delta} = {}^4\overline{\mathbb{C}}_0^{\varepsilon\phi\varphi\gamma} \overline{Q}_{\cdot\varepsilon}^{j\alpha} \overline{Q}_{\cdot\phi}^{j\beta} \overline{Q}_{\cdot\varphi}^{j\chi} \overline{Q}_{\cdot\gamma}^{j\delta}, \quad {}^6\overline{\mathbb{C}}_j^{\alpha\beta\chi\delta\varepsilon\phi} = {}^6\overline{\mathbb{C}}_0^{\varphi\gamma\eta\iota\kappa\lambda} \overline{Q}_{\cdot\varphi}^{j\alpha} \overline{Q}_{\cdot\gamma}^{j\beta} \overline{Q}_{\cdot\eta}^{j\chi} \overline{Q}_{\cdot\iota}^{j\delta} \overline{Q}_{\cdot\kappa}^{j\varepsilon} \overline{Q}_{\cdot\lambda}^{j\phi}, \quad \overline{\beta}_j^{\alpha\beta} = \overline{\beta}_0^{\chi\delta} \overline{Q}_{\cdot\chi}^{j\alpha} \overline{Q}_{\cdot\delta}^{j\beta}. \tag{39}$$

Stress–strain–temperature relations following from (27), (36), and (38) are

$$\overline{\Sigma}^{\alpha\beta} = {}^4\overline{\mathbb{C}}^{\alpha\beta\chi\delta} E_{\chi\delta}^E + \frac{1}{2} {}^6\overline{\mathbb{C}}^{\alpha\beta\chi\delta\varepsilon\phi} E_{\chi\delta}^E E_{\varepsilon\phi}^E - \overline{\beta}^{\alpha\beta}(\theta - \theta_0)$$
$$= \left[{}^4\overline{\mathbb{C}}_0^{\alpha\beta\chi\delta} E_{\chi\delta}^E + \frac{1}{2} {}^6\overline{\mathbb{C}}_0^{\alpha\beta\chi\delta\varepsilon\phi} E_{\chi\delta}^E E_{\varepsilon\phi}^E - \overline{\beta}_0^{\alpha\beta}(\theta - \theta_0) \right](1-f_T) + \sum_{j=1}^{w} \left[{}^4\overline{\mathbb{C}}_j^{\alpha\beta\chi\delta} E_{\chi\delta}^E + \frac{1}{2} {}^6\overline{\mathbb{C}}_j^{\alpha\beta\chi\delta\varepsilon\phi} E_{\chi\delta}^E E_{\varepsilon\phi}^E - \overline{\beta}_j^{\alpha\beta}(\theta - \theta_0) \right] f^j, \tag{40}$$

implying that elastic stress $\overline{\Sigma}$ for a heterogeneous (twinned) crystal is equivalent to the volume average of local stresses supported by the parent and each twin. Effective material coefficients are thus

$$ {}^4\overline{\mathbb{C}}^{\alpha\beta\chi\delta} = {}^4\overline{\mathbb{C}}_0^{\alpha\beta\chi\delta}(1-f_T) + \sum_{j=1}^{w} {}^4\overline{\mathbb{C}}_j^{\alpha\beta\chi\delta} f^j, \quad {}^6\overline{\mathbb{C}}^{\alpha\beta\chi\delta\varepsilon\phi} = {}^6\overline{\mathbb{C}}_0^{\alpha\beta\chi\delta\varepsilon\phi}(1-f_T) + \sum_{j=1}^{w} {}^6\overline{\mathbb{C}}_j^{\alpha\beta\chi\delta\varepsilon\phi} f^j,$$
$$\overline{\beta}^{\alpha\beta} = \overline{\beta}_0^{\alpha\beta}(1-f_T) + \sum_{j=1}^{w} \overline{\beta}_j^{\alpha\beta} f^j, \quad \overline{K}^{\alpha\beta} = \overline{K}_0^{\alpha\beta}(1-f_T) + \sum_{j=1}^{w} \overline{K}_j^{\alpha\beta} f^j. \tag{41}$$

From (41), necessity of inclusion of twin fractions in free energy functions (16) and (35) is evident, since effective thermoelastic coefficients depend on evolving twin fractions. For anisotropic crystals undergoing twinning, the effective matrix of thermal conductivity coefficients in (28) and (33) can be approximated in the same manner as $\overline{\beta}^{\alpha\beta}$, as indicated in the last of (41), where $\overline{K}_j^{\alpha\beta} = \overline{K}_0^{\chi\delta} \overline{Q}_{\cdot\chi}^{j\alpha} \overline{Q}_{\cdot\delta}^{j\beta}$ is the conductivity tensor of reoriented twin fraction j and $\overline{K}_0^{\chi\delta}$ is the conductivity tensor of the parent. Possible influences of dislocation densities ($\hat{\boldsymbol{\alpha}}$ and ξ) and twin boundaries (ζ) on effective elastic moduli that may arise in some crystals at large deformations and large defect densities (Smith, 1953; Chung and Clayton, 2007) are precluded by (35) since couplings between elastic strain $\mathbf{E}^E$ and defects ($\hat{\boldsymbol{\alpha}}, \xi, \zeta$) are not included. Such effects could be incorporated by generalization of (35) if deemed relevant (Clayton et al., 2004a,b). The associated rate of thermoelastic free energy change from rates of twin fractions is

$$\frac{\partial \overline{\Psi}^E}{\partial f^j} \dot{f}^j = \overline{A}_j \dot{f}^j,$$
$$\overline{A}_j = \frac{1}{2} E_{\alpha\beta}^E \left({}^4\overline{\mathbb{C}}_j^{\alpha\beta\chi\delta} - {}^4\overline{\mathbb{C}}_0^{\alpha\beta\chi\delta} \right) E_{\chi\delta}^E + \frac{1}{6} E_{\alpha\beta}^E \left({}^6\overline{\mathbb{C}}_j^{\alpha\beta\chi\delta\varepsilon\phi} - {}^6\overline{\mathbb{C}}_0^{\alpha\beta\chi\delta\varepsilon\phi} \right) E_{\chi\delta}^E E_{\varepsilon\phi}^E - \left(\overline{\beta}_j^{\alpha\beta} - \overline{\beta}_0^{\alpha\beta} \right) E_{\alpha\beta}^E (\theta - \theta_0), \tag{42}$$

with summation applied over j. Consider a situation in which strains $E_{\alpha\beta}^E = \overline{\alpha}_{\alpha\beta}(\theta - \theta_0)$ arise from temperature change. The following relationship emerges between the thermal stress, thermal expansion constants ($\overline{\alpha}_{\alpha\beta}$), and elasticity coefficients:

$$\overline{\beta}^{\alpha\beta} = {}^4\overline{\mathbb{C}}^{\alpha\beta\chi\delta} \overline{\alpha}_{\chi\delta} + \frac{1}{2} {}^6\overline{\mathbb{C}}^{\alpha\beta\chi\delta\varepsilon\phi} \overline{\alpha}_{\chi\delta} \overline{\alpha}_{\varepsilon\phi} (\theta - \theta_0), \tag{43}$$

where the second term on the right is negligible for most crystals with small coefficients $\overline{\alpha}_{\alpha\beta} \ll 1$. Symmetry conditions ${}^4\overline{\mathbb{C}}^{\alpha\beta\chi\delta} = {}^4\overline{\mathbb{C}}^{(\alpha\beta)(\chi\delta)}, {}^6\overline{\mathbb{C}}^{\alpha\beta\chi\delta\varepsilon\phi} = {}^6\overline{\mathbb{C}}^{(\alpha\beta)(\chi\delta)(\varepsilon\phi)}$, and $\overline{\beta}^{\alpha\beta} = \overline{\beta}^{(\alpha\beta)}$ follow automatically from (37). Voigt's notation (Brugger, 1964; Thurston, 1974) exploits symmetry of the elastic stress $\overline{\Sigma}$, elastic strain $\mathbf{E}^E$, and these elastic coefficients, where pairs of indices $11 \to 1, 22 \to 2, 33 \to 3, 23 \to 4, 13 \to 5$, and $12 \to 6$, and $\overline{\Sigma}^{\alpha\beta} \to \overline{\Sigma}_A, 2E_{\alpha\beta}^E \to E_A^E(1 + \delta_{\alpha\beta})$, where $\alpha, \beta = 1,2,3$ and $A = 1,2,\ldots 6$. Relations between stress, strain, and temperature change in (40) then can be expressed compactly as

$$\overline{\Sigma}_A = C_{AB} E_B^E + \frac{1}{2} C_{ABC} E_B^E E_C^E - \overline{\beta}_A (\theta - \theta_0), \tag{44}$$

where C_{AB} and C_{ABC} are second- and third-order elastic coefficients written in the standard notational scheme of Brugger (1964) and summation proceeds over duplicate covariant indices. Thermal energy in (35) is prescribed as (Clayton, 2005, 2009)

$$\overline{Y} = -\overline{c}\theta \ln(\theta/\theta_0). \tag{45}$$

Finally, the residual energy of lattice defects in (35) is specified as

$$\overline{\Psi}^R = \frac{1}{2}\mu\left[\kappa_1\xi^2 + \kappa_2\zeta^2 + \kappa_3 l^{2N}(\hat{\boldsymbol{\alpha}}:\hat{\boldsymbol{\alpha}})^N + \kappa_4\xi^2\zeta^2 + \kappa_5 l^{2N}(\hat{\boldsymbol{\alpha}}:\hat{\boldsymbol{\alpha}})^N\xi^2 + \kappa_6 l^{2N}(\hat{\boldsymbol{\alpha}}:\hat{\boldsymbol{\alpha}})^N\zeta^2\right], \tag{46}$$

where μ is an elastic shear modulus that may depend on temperature and $\kappa_1, \kappa_2, \ldots \kappa_6$ are dimensionless constants that scale energies associated with internal state variables. The proper choice of μ for anisotropic materials is discussed in Appendix C. Also, l is scalar with dimensions of length, required from dimensional considerations in gradient theories (Fleck et al., 1994; Bammann, 2001; Regueiro et al., 2002; Abu Al-Rub and Voyiadjis, 2004; Clayton et al., 2004a,b), and N is a constant. Recalling from Section 3.1 that $\xi = b\sqrt{\rho_S}$, the first term on the right of (46) provides a linear dependence of residual energy on the line density of statistically stored dislocations, following Bammann (2001), Regueiro et al. (2002), Clayton et al. (2004a, 2006), and references therein. Simple arguments lead to $2E_\rho = \kappa_1\mu b^2$, where E_ρ is the total energy per unit line length of statistically stored dislocations, including self- and interaction energies, core energy, and stacking fault energy if the dislocations are partial. Recalling that $\zeta = \sqrt{b\eta_T}$, the second term provides for a linear dependence of residual energy on the area per unit volume of twin boundaries η_T. Similarly, $2E_T = \kappa_2\mu b$, where E_T is the twin boundary energy per unit area. In many crystals, $2E_T \approx W_{SF}$, where W_{SF} is the intrinsic or extrinsic stacking fault energy (Hirth and Lothe, 1982; Bernstein and Tadmor, 2004). The third term accounts for the total line and interaction energy of geometrically necessary dislocations, for which a number of forms for l, N, and κ_3 have been suggested for different materials and applications (Fleck et al., 1994; Regueiro et al., 2002; Abu Al-Rub and Voyiadjis, 2004; Clayton et al., 2004a; Chung and Clayton, 2007). The fifth term accounts for interaction energies between statistically stored and geometrically necessary dislocations. The fourth and sixth terms in (46) reflect interaction energies between twin boundaries and dislocations, for example energies of dislocation lines may be amplified at the stress concentration caused by a pile-up at a twin boundary (Christian and Mahajan, 1995).

Methods for determining content of geometrically necessary versus statistically stored dislocations have been forwarded in recent years (Arsenlis and Parks, 1999; El-Dasher et al., 2003; Hughes et al., 2003), which could facilitate unique selection of parameters in (46) if defect energies are known. For example, energies can be determined through measurements of cold work (Clarebrough et al., 1957; Taheri et al., 2006) or atomic simulations of defect energy (Chung and Clayton, 2007). However, in many cases, only the total scalar line density ρ_T of all dislocations, both geometrically necessary and statistically stored, may be known from historical data. In such cases, it becomes prudent to employ a reduced form of (46) written in terms of ρ_T:

$$\overline{\Psi}^R = \frac{1}{2}\mu\left(\kappa_1\hat{\xi}^2 + \kappa_2\zeta^2 + \kappa_4\hat{\xi}^2\zeta^2\right), \tag{47}$$

with $\hat{\xi} = b\sqrt{\rho_T}$. Comparison of (46) and (47) implies

$$\rho_T = \rho_S + \rho_G, \quad \rho_G = b^{-1}(\hat{\boldsymbol{\alpha}}:\hat{\boldsymbol{\alpha}})^{1/2}, \quad l = b, \quad N = 1/2, \quad \kappa_1 = \kappa_3, \quad \kappa_4 = \kappa_6, \quad \kappa_5 = 0. \tag{48}$$

Relations (48) provide for an equal contribution, per line length, of geometrically necessary and statistically stored dislocations to the free energy. For uniform straight dislocations of density ρ^i with identical Burgers vectors, (15) and (48) consistently give $\rho_G = b^{-1}(\rho^i b^\alpha \varsigma^\beta \rho^i b_\alpha \varsigma_\beta)^{1/2} = \rho^i b^{-1}(b^\alpha b_\alpha)^{1/2}$. Using (35) and (47), the rate of temperature increase in (33) can be written[1]

$$\bar{c}\dot{\theta} = \beta'W^P + \theta\left(\frac{\partial\overline{\Psi}}{\partial\theta}\frac{\dot{J}}{J} - \overline{\boldsymbol{\beta}}:\dot{\mathbf{E}}^{\mathbf{E}}\right) + \overset{\vee}{\nabla}\cdot\overline{\mathbf{K}}\nabla\theta, \tag{49}$$

where

$$\beta' = 1 - \left\{\left[\mu - \theta\frac{\partial\mu}{\partial\theta}\right]\left[\frac{b^2}{2}\left(\kappa_1 + \kappa_4\frac{\eta_T}{\sqrt{\rho_T}}\right)\dot{\rho}_T + \frac{b}{2}\left(\kappa_2 + \kappa_4 b^{3/2}\frac{\rho_T}{\sqrt{\eta_T}}\right)\dot{\eta}_T\right] + \left[\overline{A}_j - \theta\frac{\partial\overline{A}_j}{\partial\theta}\right]\dot{f}^j\right\}W^{P-1} \tag{50}$$

is the Taylor–Quinney parameter (Taylor and Quinney, 1934; Clayton, 2005), such that $1 - \beta'$ is the ratio of inelastic stress power $W^P = \overline{\boldsymbol{\Pi}}:[\mathbf{L}^{\mathbf{I}} + \overline{\mathbf{L}}^{\mathbf{P}} + (1/3)\overline{J}\overline{J}^{-1}\mathbf{1}]$ converted to stored energy. Definition (50) is framed in terms of the total dislocation density. A more specific form of (50) accounting for distinct contributions from geometrically necessary and statistically stored dislocations can be determined in a straightforward manner by substituting (35) and (46) into (33).

3.5. Kinetics

Rate dependent, i.e., viscoplastic, kinetic laws are suggested to describe shearing from slip (Hutchinson, 1976; Teodosiu and Sidoroff, 1976; Asaro, 1983) and twinning (Wu et al., 2007):

$$\dot{\gamma}^i = \dot{\gamma}_S\left|\frac{\overline{\tau}^i}{\overline{g}^i}\right|^m\frac{\overline{\tau}^i}{|\overline{\tau}^i|}, \quad \dot{\gamma}_j^i = \dot{\gamma}_S\left|\frac{\overline{\tau}_j^i}{\overline{g}_j^i}\right|^m\frac{\overline{\tau}_j^i}{|\overline{\tau}_j^i|}, \quad \dot{f}^j = \frac{\dot{\gamma}_T}{\gamma^j}\left|\frac{\langle\overline{\tau}^j\rangle}{\overline{g}^j}\right|^p. \tag{51}$$

---

[1] In a previous paper (Clayton, 2009), an incorrect factor of 3 preceded $\overline{J}$ in the denominator of (49). That misprint is corrected here and is consistent with (33), which has also been corrected in a similar manner.

In (51), $\dot{\gamma}_S$ and $\dot{\gamma}_T$ are material parameters with dimensions of $1/t$, m and p are dimensionless parameters, and $\overline{g}^i$ and $\overline{g}^j$ are evolving resistances—positive scalars with dimensions of stress—to deformation in the parent grain by slip on system i and twinning on system j, respectively. In the second of (51), $\overline{g}^i_j$ denotes resistance on slip system i within reoriented twin j. In the third of (51), $2\langle\overline{\tau}^j\rangle = \overline{\tau}^j + |\overline{\tau}^j|$. From (30) and (51), these rates are always thermodynamically dissipative since for each slip system, $\overline{\tau}^i\dot{\gamma}^i \geqslant 0$ and $\overline{\tau}^i_j\dot{\gamma}^i_j \geqslant 0$, and since for each twin, the product $\dot{f}^j\overline{\tau}^j\gamma^j \geqslant 0$. Because $\dot{f}^j = 0$ for $\overline{\tau}^j \leqslant 0$, the unidirectional nature of twinning is respected. In the limit $m \rightarrow \infty$ or $p \rightarrow \infty$, rate independent behavior is attained, respectively, for slip or twinning. In a general sense, slip and twin resistances evolve as

$$
\begin{aligned}
\dot{\overline{g}}^i &= \dot{\overline{g}}^i\Big(\mathbf{E}^\mathbf{E}, \theta, \hat{\boldsymbol{\alpha}}, \xi, \zeta, \{f^j\}, \{\overline{g}\}\Big), \\
\dot{\overline{g}}^i_j &= \dot{\overline{g}}^i_j\Big(\mathbf{E}^\mathbf{E}, \theta, \hat{\boldsymbol{\alpha}}, \xi, \zeta, \{f^j\}, \{\overline{g}\}\Big), \\
\dot{\overline{g}}^j &= \dot{\overline{g}}^j\Big(\mathbf{E}^\mathbf{E}, \theta, \hat{\boldsymbol{\alpha}}, \xi, \zeta, \{f^j\}, \{\overline{g}\}\Big),
\end{aligned}
\tag{52}
$$

where the rates depend not only on the set of state variables that explicitly enter the free energy (16), but also on the set of hidden variables $\{\overline{g}\} = \left\{\overline{g}^i, \overline{g}^j, \overline{g}^i_j\right\}$ with $i = 1, \ldots n$ and $j = 1, \ldots w$, consisting of all possible slip and twinning resistances. Slip and twin resistances $\{\overline{g}\}$ are also referred to as flow stresses. Residual volume change $\overline{J} = \overline{J}(\theta, \hat{\boldsymbol{\alpha}}, \xi, \zeta, \{f^j\})$ depends on defect content and temperature, the latter dependence a result of temperature influences on the elastic coefficients and their pressure derivatives. Specific formulae quantifying $\overline{J}$ are deferred to (65)–(67) in Section 4.4.

Evolution equations for scalar internal state variables ξ and ζ, reflecting respective densities of statistically stored dislocations and twin boundaries, complete the model. An explicit evolution equation for the geometrically necessary dislocation tensor is not needed since $\hat{\boldsymbol{\alpha}}$ follows directly from kinematic definition (15). Analogous to hardening in (51), defect densities may depend upon history of slip and twin activity, as well as crystal structure and material composition. Generic evolution equations are

$$
\dot{\xi} = \dot{\xi}\Big(\mathbf{E}^\mathbf{E}, \theta, \hat{\boldsymbol{\alpha}}, \xi, \zeta, \{f^j\}, \{\overline{g}\}\Big), \quad \dot{\zeta} = \dot{\zeta}\Big(\mathbf{E}^\mathbf{E}, \theta, \hat{\boldsymbol{\alpha}}, \xi, \zeta, \{f^j\}, \{\overline{g}\}\Big).
\tag{53}
$$

From (52) and (53), free energy (16) thus depends on hidden variables $\{\overline{g}\}$ implicitly, via their influence on evolution of the state variables.

Possible impedance or facilitation of slip or twinning via slip–slip interactions, slip–twin interactions, and twin–twin interactions depends in a complex manner on a number of factors, including geometrical relationships between interacting systems, temperature, crystal structure, and defect content (Christian and Mahajan, 1995; Lu et al., 1998; Castaing et al., 2002; Wu et al., 2007). Experimental data enabling unique quantification of these effects is often scarce, and mechanisms responsible for hardening are not fully understood in many materials (Lagerlof et al., 1994). Because of the large number of parameters required for a complete description of interactions between individual deformation mechanisms, many experiments may be required, with delineation of effects of a particular mechanism difficult. Initial values of hardness in (52) may differ among different slip and twin families in a crystal, and may account for periodic lattice resistance in an initially perfect crystal (Peierls, 1940; Nabarro, 1947), friction stress (Beltz et al., 1996), and other initial barriers, for example those resulting from interstitials in crystals with impurities (Kocks et al., 1975). Short range barriers to dislocation motion are often strongly temperature-dependent (Kuhlmann-Wildsorf, 1960; Kocks et al., 1975), since increases in temperature correlate with increased probability of dislocations overcoming such barriers via thermal activation. Long range barriers typically arise from interactions of local stress fields between defects, and generally increase with defect densities that tend to accumulate with strain until saturation. Twinning resistance is often affected by temperature, and at low temperatures may increase less steeply than slip resistance as the temperature is decreased (Christian and Mahajan, 1995). This phenomenon explains the tendency for some solids to favor twinning over slip at low temperatures. Resistance to twinning may even decrease with decreasing temperature (Christian and Mahajan, 1995). Recent models addressing slip, twinning, and slip-twin interactions via detailed hardening laws were advanced by Beyerlein and Tomé (2008), Proust et al. (2009), Shiekhelsouk et al. (2009). Proust et al. (2009) also modeled mechanical detwinning.

The present model assumes that thermoelastic deformation (and hence elastic strain) is uniform over the parent and all twins comprising a volume element at a given "material point", as is clear from developments in Section 3.4. Such an approach, whereby the total stress at a material point is a volume average of stresses in parent and individual twins, is similar to earlier models of Kalidindi (1998, 2001). Advantages and disadvantages of this type of approach are discussed by Proust et al. (2007). Specifically, the present approach allows for straightforward application of hardening laws such as (52). However, secondary twinning and detwinning are not addressed in the present model. Furthermore, stress equilibrium among twinned and parent regions with different anisotropic elastic constants is not strictly maintained according to the present model. Alternative approaches accounting for various equilibrium and compatibility constraints have been formulated, using micromechanics arguments, for crystals with lamellar structures (Lebensohn, 1999; Proust et al., 2007). Self-consistent models have also been applied to anisotropic polycrystals with hexagonal (Lebensohn and Tomé, 1993) and trigonal (Tomé et al., 1991b) symmetry. It is noted that the present theory is intended to be applied at material points associated with a small length scale within a single crystal, and no assumptions are made regarding interactions among grains in a polycrystal. The present model also includes a number of features often absent in other treatments: thermodynamics of heat conduction

or adiabatic temperature rise, thermal expansion, higher-order elastic constants, internal state variables associated with energies of lattice defects such as dislocations and stacking faults, and possible volume changes induced by defects.

4. Application: corundum single crystals with impurities

The framework of Section 3 is specialized in Section 4 to describe elasticity and inelasticity in pure and doped corundum. Crystal structure and properties, yield mechanisms, strain hardening, defect accumulation, and residual volume changes are considered. Initial yield mechanisms are addressed for pure alumina single crystals over a range of temperatures, and for doped corundum at high temperatures. The quantitative treatment of strain hardening and defect accumulation focuses first on pure and doped corundum deformed by basal glide at high temperatures. New predictions are then provided for rhombohedral twinning and for basal double slip followed by rhombohedral twinning in pure corundum. New comparisons of model features to results of atomic calculations performed elsewhere are reported.

Some discussion in Sections 4.1 and 4.2 is abbreviated from a previous paper (Clayton, 2009), wherein a more complete description of properties of pure alumina single crystals was given, and other calculations of the response of pure single crystals of various orientations to impact loading were reported. Discussion and corresponding tables and figures in Sections. 4.3 and 4.4 contain refinements to the previous model of pure corundum (Clayton, 2009), new results for basal slip and defect-induced volume changes in doped corundum, and new treatment of twin boundaries. Comparisons with atomic model results in Section 4.5 are also new.

4.1. Crystal structure and properties

The atomic structure of pure α-corundum is depicted in Fig. 3, following Kronberg (1957). The primitive unit cell is rhombohedral (two formula units per cell, lattice parameter $a_0 = 0.512$ nm, bond angle 55.3°). The hexagonal unit cell, while consisting of more atoms (six formula units per cell), is more convenient for describing mechanical behavior. Two types of hexagonal cells are encountered in the literature (Kronberg, 1957). One is the morphological cell shown in Fig. 3, with lattice parameters $A_1 = 0.475$ nm and $C_M = 0.649$ nm. The second is the structural cell, consisting of a second stack of each of three layers of Al cations and O anions, differing from the morphological unit cell by a rotation of 180° about the *c*-axis [0001]. Parameters of the structural hexagonal cell are $A_1' = 0.475$ nm and $C_S = 2C_M = 1.297$ nm, shown in Fig. 4. Elastic constants are listed in Table 1. In Table 1 and henceforth, all anisotropic properties are referred to the structural unit cell. Relevant bulk physical properties with supporting references are listed in Table 2.

Prominent slip and twin systems are listed in Tables 3 and 4, respectively, and are illustrated in Fig. 4. While basal and prism slip can occur in either direction for a given system, pyramidal slip is thought unidirectional (Heuer et al., 1998) and only occurs when the resolved shear stress acts in a positive sense with respect to the *c*-axis, e.g., tensile loading along [0001]. Twinning is also unidirectional; for example, rhombohedral twinning occurs only when the resolved shear stress acts in a negative sense with respect to the *c*-axis, such as occurs in compressive loading along [0001]. Thus, pure tensile deformation along [0001] can only be accommodated by pyramidal slip, elasticity, or fracture, while pure compression along [0001] can only be accommodated by rhombohedral twinning, elasticity, or fracture. Slip directions for unidirectional
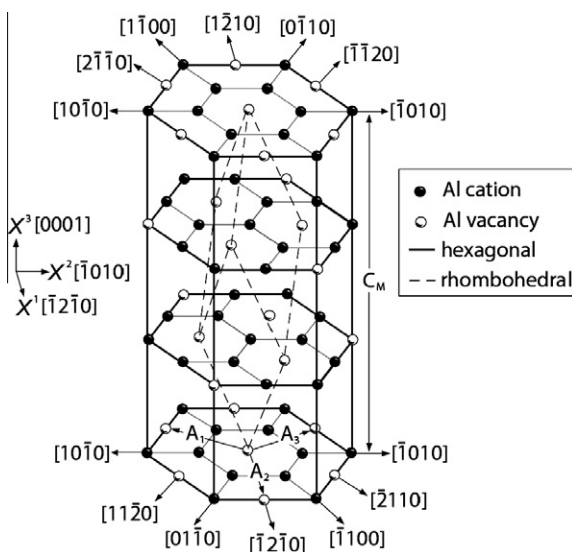

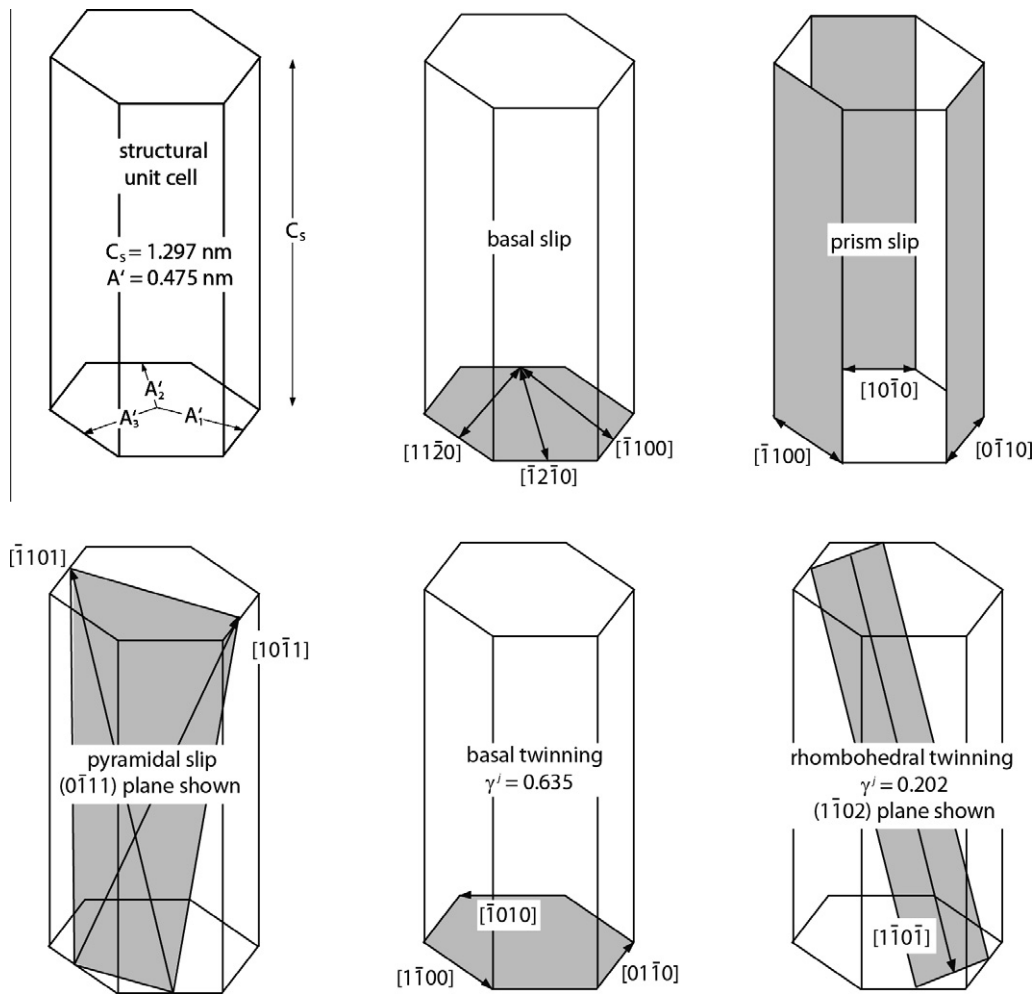**Fig. 3.** Morphological unit cell of sapphire (Kronberg, 1957).

Fig. 4. Prominent slip and twin systems in corundum (structural unit cell notation).

Table 1
Elastic coefficients at room temperature.

Parameter	Value [GPa][a]	Parameter	Value [GPa][a]	Parameter	Value [GPa][a]
C_{11}	498	C_{111}	−3780	C_{134}	131
C_{12}	163	C_{112}	−1090	C_{144}	−302
C_{13}	117	C_{113}	−963	C_{155}	−1160
C_{14}	23	C_{114}	−55	C_{222}	−4520
C_{33}	502	C_{123}	−289	C_{333}	−3340
C_{44}	147	C_{124}	39	C_{344}	−1090
		C_{133}	−922	C_{444}	19

[a] Winey et al. (2001).

mechanisms are tabulated here such that the resolved shear stress for that slip or twin system must be positive to enact shear on that system. Bourne et al. (2007) observed prism and basal dislocations, twins, cleavage fracture, and grain boundary fracture in specimens recovered from impact experiments on polycrystalline alumina, with activity or inactivity of certain mechanisms dependent on the impact stress. Atomistic simulations of hypervelocity impact of sapphire have also predicted basal and pyramidal slip and basal and rhombohedral twinning (Zhang et al., 2007, 2008). Quantification of resistances for slip, twinning, and fracture in corundum is currently an area of active research (Tymiak and Gerberich, 2007; Clayton, 2009; Tymiak et al., 2009). Because of alumina's brittleness at low temperatures, experimental measurements of yield mechanisms at low temperatures must occur at high pressures that suppress tensile fracture, e.g., indentation (Tymiak and

Table 2
Bulk physical properties (atmospheric pressure).

Parameter	Value	Remarks
ρ_0	3980 kg/m^3	Room temperature mass density[a]
c	$780 + 0.3(\theta - 300)$ J/kg K	Specific heat per unit mass[b]
$\overline{\alpha}_{11}$	5.0×10^{-6}/K	Thermal expansion coefficient[a]
$\overline{\alpha}_{33}$	5.7×10^{-6}/K	Thermal expansion coefficient[a]
θ_M	2325 K	Melting temperature[b]
$\overline{K}$	30 W/mK	Thermal conductivity[c] (300 K)
μ	$156 - 70(\theta/\theta_M)$ GPa	Rhombohedral shear modulus (C_{44})[d]

[a] Burghartz and Schulz (1994).
[b] Castanet (1984).
[c] Cahill et al. (1998).
[d] Zouboulis and Grimsditch (1991).

Table 3
Slip systems and slip dislocations.

Type	Direction	Plane	Burgers vector[a]	b [nm]	Remarks
Basal	$[11\bar{2}0]$	(0001)	$1/3[11\bar{2}0]$	0.475	Bidirectional[b]
	$[\bar{1}2\bar{1}0]$	(0001)			
	$[\bar{2}110]$	(0001)			
Prism	$[1\bar{1}00]$	$(11\bar{2}0)$	$1/3[1\bar{1}00]$	0.274	Bidirectional[b]
	$[10\bar{1}0]$	$(\bar{1}2\bar{1}0)$			
	$[01\bar{1}0]$	$(\bar{2}110)$			
Pyramidal	$[\bar{1}101]$	$(10\bar{1}1)$	$1/3[\bar{1}101]$	0.512	Unidirectional[c]
	$[0\bar{1}11]$	$(10\bar{1}1)$			
	$[10\bar{1}1]$	$(0\bar{1}11)$			
	$[\bar{1}101]$	$(0\bar{1}11)$			
	$[0\bar{1}11]$	$(\bar{1}101)$			
	$[10\bar{1}1]$	$(\bar{1}101)$			

[a] Kronberg (1957), Tressler and Barber (1974), and Lagerlof et al. (1994).
[b] Kronberg (1957), Snow and Heuer (1973), and Heuer et al. (1998).
[c] Tressler and Barber (1974).

Table 4
Twin systems, partial dislocations, and stacking fault energies.

Type	Direction	Plane	Shear	Burgers vector[a]	b [nm]	W_{SF} [J/m^2]
Basal (type II[b])	$[\bar{1}010]$	(0001)	0.635	$1/3[\bar{1}010]$	0.274	1.2–6.7[d]
	$[1\bar{1}00]$	(0001)				
	$[01\bar{1}0]$	(0001)				
Rhombohedral (type I[c])	$[\bar{1}01\bar{1}]$	$(\bar{1}012)$	0.202	$1/21.9[1\bar{1}0\bar{1}]$	0.071	0.25[e]
	$[01\bar{1}\bar{1}]$	$(01\bar{1}2)$				
	$[1\bar{1}0\bar{1}]$	$(1\bar{1}02)$				

[a] Kronberg (1957), Geipel et al. (1994), and Heuer et al. (1998).
[b] Veit (1921) and Kronberg (1957).
[c] Heuer (1966).
[d] Kenway (1993) and Marinopoulos and Elsasser (2001).
[e] Lagerlof et al. (1984).

Gerberich, 2007; Tymiak et al., 2009) or confined compression (Graham and Brooks, 1971; Castaing et al., 1981; Scott and Orr, 1983; Lankford et al., 1998).

4.2. Yield in corundum

Flow stresses $\{\overline{g}\}$ entering (51)–(53) are decomposed into sums of contributions of various mechanisms, e.g., following Kocks et al. (1975) and Clayton (2005, 2009):

$$\overline{g}^i = g_S^i + g_L^i, \quad \overline{g}_j^i = g_{jS}^i + g_{jL}^i, \quad \overline{g}^j = g_S^j + g_L^j. \tag{54}$$

Here, $g_S^i = \overline{g}_{t=0}^i$ reflects the initial yield stress for slip in the parent crystal on system i, and g_L^i reflects long-range barriers associated with defects that accumulate during the deformation history. Analogous definitions apply for resistance to slip within the twins and resistance to twin propagation in the second and third of (54), respectively. Both terms in each sum in (54) depend on temperature; the first, i.e., initial yield, is reviewed here for commercially pure corundum over a range of temperatures, following Clayton (2009). Such a review is necessary to provide sufficient background for the discussion of new results given in Sections. 4.3 and 4.4. The second term on the right side of the first equality in (54), g_L^i, is newly addressed in Section 4.3 for pure and doped alumina deformed plastically at high temperatures.

The initial yield stress depends on short range barriers such as strong Peierls barriers in crystals with low initial defect densities and non-metallic bonds (Friedel, 1964; Farber et al., 1993), and at high rates also accounts for viscous, phonon, and electron drag (Kocks et al., 1975; Gilman, 1979). Short range barriers exhibit a strong dependence on temperature for both slip and twinning in sapphire (Lagerlof et al., 1994), reflected appropriately by

$$g_S^i = g_0^i \exp\left(-\lambda^i \frac{\theta}{\theta_M}\right), \quad g_S^j = g_0^j \exp\left(-\lambda^j \frac{\theta}{\theta_M}\right), \tag{55}$$

where g_0^i is an athermal yield stress, θ_M is the melting temperature, and λ^i is a dimensionless parameter. Analogous definitions apply for quantities associated with twin system j in the second of (55). Appropriate forms for the temperature dependence of the second of (54), i.e., for slip systems within twinned regions, have not been verified experimentally for sapphire, but it may be reasonable to assume that short range barriers for a slip system in the parent are transferred to its rotated counterpart in a twinned region. Relation (55) does not conform to the usual Arrhenius form for thermally activated kinetics (Kocks et al., 1975) but can be justified physically in terms of activation volumes for cross-slip in alumina (Lagerlof et al., 1994). Values of g_0 and λ are compiled in Table 5 for pure alumina crystals for mechanisms of basal, prism, and pyramidal slip and basal and rhombohedral twinning. Comparisons to experimental data are provided in Fig. 5 (Clayton, 2009). Room temperature experimental values follow from nonlinear elasticity calculations of driving forces for inelastic shearing mechanisms operative at the experimental HEL in single crystals of various orientations (Clayton, 2009) or from values appropriate for indentation (Tymiak and Gerberich, 2007). High temperature data for basal and prism glide are obtained from Lagerlof et al. (1994). Data for pyramidal slip are obtained from Tressler and Barber (1974). For basal twinning, data are obtained from Castaing et al. (2004), and for rhombohedral twinning, from Scott and Orr (1983). For rhombohedral twinning, the fits are most appropriate for $300 \leqslant \theta \leqslant 1300$ K, for basal twinning most valid for $300 \leqslant \theta \leqslant 1600$ K, and for slip the model validly spans the range $300 \leqslant \theta \leqslant 2100$ K. Trend lines extended to the lower limit $\theta = 0$ K are extrapolations. Strain rate dependence of twinning is not thought to be significant, based on experimental observations (Scott and Orr, 1983). Rate sensitivities of pyramidal slip with $m \approx 10$ (Tressler and Barber, 1974) and prism slip with $m \approx 16$ (Castaing et al., 1981) have been observed for sapphire deformed at low rates and high temperatures. Pressure and rate dependence are not considered in Fig. 5 but could be included in a more refined model when supporting experimental data spanning a wide range of pressures and strain rates become available for all slip and twin families. Predictions at a temperature of 300 K follow the sequence

$$g_S^{\text{pyramidal slip}} > g_S^{\text{basal twin}} \approx g_S^{\text{basal slip}} > g_S^{\text{prism slip}} > g_S^{\text{rhombohedral twin}}, \tag{56}$$

in general agreement with trends for slip resistances in indentation (Tymiak and Gerberich, 2007).

4.3. High temperature hardening and defect accumulation in pure and doped alumina

Conceivably, long-range barriers in each of (54) could depend in a complex manner upon activity of the slip or twin system under consideration (i.e., self-hardening) as well as the activity of all other slip systems (i.e., latent hardening) and twin systems (Christian and Mahajan, 1995; Wu et al., 2007). Considered here are phenomena for which supporting experimental data are available: hardening of basal slip and hardening of rhombohedral twinning by total dislocation line accumulation.

Table 5
Slip and twinning parameters for commercially pure alumina.

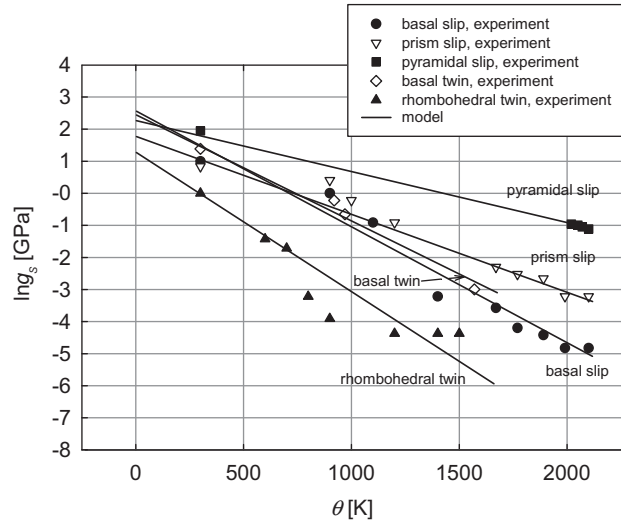| Parameter	Value	Remarks	Parameter	Value	Remarks
g_0 [GPa]	12.7	Basal slip	g_m [GPa]	53.6	Basal slip
	6.6	Prism slip	ω	10.7	Basal slip
	10.0	Pyramidal slip	h_0	8.0×10^{-3}	Basal slip
	11.5	Basal twin	h_1	9.3×10^{-3}	Basal slip
	3.4	Rhombohedral twin	α_0	0.54	Basal slip
λ	8.4	Basal slip	α_1	0.64	Basal slip
	5.6	Prism slip	h_R	0.58	Rhombohedral twin
	3.7	Pyramidal slip			
	7.7	Basal twin			
	10.2	Rhombohedral twin			

Fig. 5. Shear stresses for initial yield by slip or twinning in pure corundum (Clayton, 2009).

Addressing first the hardening of slip systems, i.e., the glide resistance, the rate of resistance to long-range barriers in (54) is prescribed as

$$\dot{g}_L^i = \left(1 - \frac{g_L^i}{g_M^i}\right) h^i \sum_{k=1}^{n} |\dot{\gamma}^k|, \quad g_L^i|_{t=0} = 0, \tag{57}$$

where g_M^i is a saturation stress (Wu et al., 2007) and h^i is a hardening modulus. These quantities depend on the thermodynamic state of the crystal as follows:

$$g_M^i = g_m^i \exp\left(-\omega^i \frac{\theta}{\theta_M}\right), \quad h^i = \mu\left(h_0^i - h_1^i \frac{\theta}{\theta_M}\right), \tag{58}$$

where g_m^i, ω^i, h_0^i, and h_1^i are material constants that may differ among different families of slip systems. These constants, as well as g_0 of (55), may also vary with the concentration of impurities or dopants (Klassen-Neklyudova et al., 1970; Pletka et al., 1982). For example, substitutional atoms such as Cr, Ti, and Mg may be present in natural (e.g., geologic) crystals, or may be added to a synthetic ceramic to adjust its mechanical, electrical, and/or optical properties (Castaing et al., 2002).

Relations (57) and (58) provide a reasonable fit to the experimental basal slip data of Pletka et al. (1977) for pure sapphire over the range $1673 \leqslant \theta \leqslant 1993$ K, as shown in Fig. 6(a), with model parameters listed in Table 5. In Fig. 6, γ^P is the cumulative plastic shear from glide on a single system. As shown in Fig. 6(b), the model accurately describes the response of corundum doped with cations of Cr^{3+}, Ti^{3+}, Ti^{4+}, or Mg^{2+}; atomic percentages of each dopant and corresponding hardening parameters are listed in Table 6. For pure alumina and all doped variants, $\lambda = 8.4$ of Table 5 is used. For all model predictions and experimental results (Pletka et al., 1982) shown in Fig. 6(b) except those for Cr^{3+} doping, the temperature is $\theta = 1793$ K. For Cr^{3+}-doped corundum, predictions and experimental results (Pletka et al., 1982) of Fig. 6(b) correspond to $\theta = 1773$ K.

As is clear in Fig. 6(a), model predictions do not provide an ideal fit to all experimental data. For example, dips in experimentally observed shear stresses at plastic shear strains on the order of a few percent are not captured by the model of (57) and (58). Pletka et al. (1977) attributed such dips to an increase in mobile dislocation density associated with dislocation sources and dipole break-up. Furthermore, the saturation stress at large plastic shear strain is not predicted accurately for all temperatures; e.g., the model fit is excellent at 1773 K for $\gamma^P \geqslant 0.20$, while the saturation stress is under-predicted by the model by at least 20% at 1673 K. The law used for temperature dependence of glide resistance in the present model has been selected as a compromise between simplicity (exponential and linear forms in (58), four parameters) and accuracy. More accurate temperature-dependent hardening/softening laws could always be attempted at the possible expense of additional model complexity and added fitting parameters.

Dislocation accumulation takes place in conjunction with slip system hardening according to

$$g_L^i = \alpha^i \mu b(\sqrt{\rho_T} - \sqrt{\rho_{T0}}), \quad \alpha^i = \alpha_0^i - \alpha_1^i \frac{\theta}{\theta_M}, \tag{59}$$

where ρ_{T0} is the initial dislocation density and α_0^i and α_1^i are dimensionless constants that may vary among families of slip systems. Following Pletka et al. (1977), (59) extends the theory of Taylor (1934) of slip impedance from dislocation interactions on parallel planes to conditions wherein the ratio between shear strength and dislocation density decreases with increasing temperature. Relation (59) improves on a previous relation (Clayton, 2009) that did not allow $\rho_T < \rho_{T0}$ as may
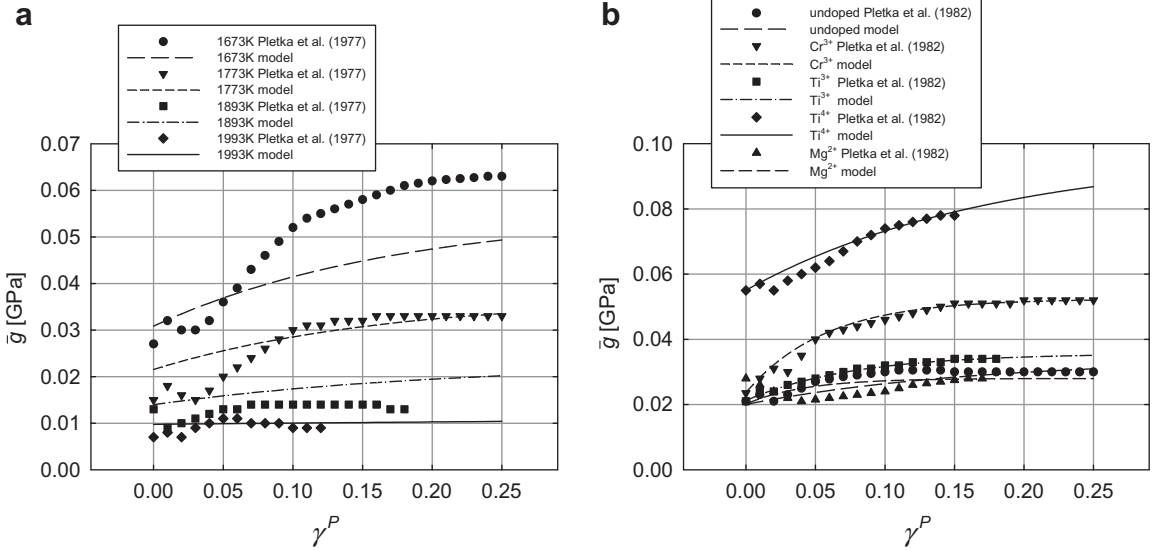
Fig. 6. Shear stresses for slip on the basal plane: (a) pure alumina over range of temperatures and (b) pure and doped alumina at $\theta \approx 1800$ K.

Table 6
Basal slip parameters for doped alumina (≈ 1800 K).

Dopant	Atomic %[a]	g_0 [GPa]	g_m [GPa]	h_0	h_1	α
Cr^{3+}	0.20	14.0	100	1.2×10^{-2}	9.3×10^{-3}	0.150
Ti^{3+}	0.047	13.5	55	9.0×10^{-3}	9.3×10^{-3}	0.067
Ti^{4+}	0.047	35.0	160	9.5×10^{-3}	9.3×10^{-3}	0.15
Mg^{2+}	0.002	12.8	30	9.0×10^{-3}	9.3×10^{-3}	-0.12

[a] Pletka et al. (1982).

result from dislocation annihilation. Parameters are listed in Table 5 for pure alumina, following calibration to data obtained over the temperature range $1673 \leqslant \theta \leqslant 1993$ K from basal slip experiments at a rate of $\dot{\gamma}^p \approx \dot{\gamma}_S = 1.33 \times 10^{-4}$/s (Pletka et al., 1977). Values of α_0 and α_1 listed in Table 5 differ from those listed previously (Clayton, 2009) as a result of new relation (59). Predictions are compared with data (Pletka et al., 1977) for pure sapphire in Fig. 7(a). Predictions of the model are compared with data (Pletka et al., 1982) for doped corundum deformed by basal glide at temperatures $\theta \approx 1800$ K in Fig. 7(b). Parameter α is listed in Table 6 for each doped variant of alumina, valid at $\theta \approx 1800$ K. Additional experiments at various temperatures are required to determine the temperature dependence of α in the second of (59) for each of the doped variants. From Fig. 7, dislocation densities increase with plastic shear strain from initial value $\rho_{T0} = 10^8$ m^{-2} (Pletka et al., 1977) to saturation values in the range 10^{12} m$^{-2} < \rho_T < 10^{14}$ m^{-2} that increase with decreasing temperature.

When all systems in a given family harden equally (Taylor, 1934), for example as in (57), relation (59) can be inverted and used with (57) to provide an evolution equation for the total accumulated dislocation density (Clayton, 2005). Generalization of (57)–(59) is required to account for potentially more complex interactions between active and inactive systems (i.e., self-hardening versus latent hardening), and for interactions between statistically stored and geometrically necessary dislocations (Rezvanian et al., 2007). Both h^i of (58) and g_L^i of (59) are scaled consistently by the rhombohedral shear modulus μ that depends on temperature (Table 2 and Appendix C).

Experiments also provide quantitative evidence for hardening of rhombohedral twin propagation by accumulation of forest dislocations (Castaing et al., 2002). Such behavior is captured by

$$\dot{g}_L^j = \sum_{i=1}^{n} h_i^j \dot{g}_L^i, \quad g_L^j \big|_{t=0} = 0, \tag{60}$$

where slip on all systems can contribute to the hardness of twin system j, and h_i^j is an interaction matrix relating the hardening rate of slip system i to that of twin fraction j. Setting $h_i^j = h_R$ for all basal slip systems i and rhombohedral twin systems j gives $\dot{g}_L^j = h_r \sum_i \dot{g}_L^i$ with the value of h_R listed in Table 5, fit to data of Castaing et al. (2002) for hardening of rhombohedral twinning by basal slip.

Rhombohedral twinning is considered quantitatively in Fig. 8(a). Loading conditions in Fig. 8(a) correspond to uniaxial compressive stress applied normal to the basal plane (i.e., parallel to the c-axis). For such conditions, the only operative
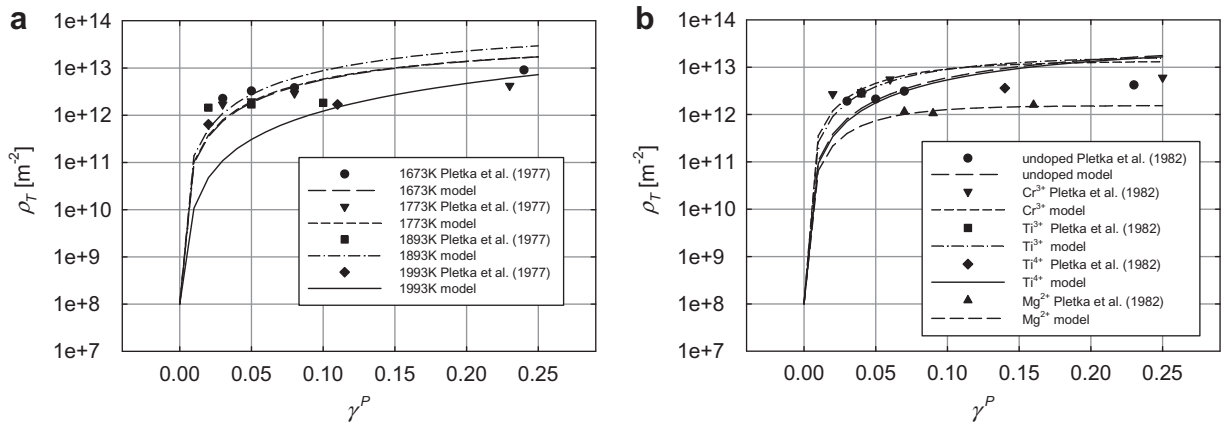
Fig. 7. Dislocation density accumulation from slip on the basal plane: (a) pure alumina over range of temperatures and (b) pure and doped alumina at $\theta \approx 1800$ K.

inelastic deformation mechanism is rhombohedral twinning, which can occur simultaneously on any of the three rhombo-hedral twin systems of Table 4, each with a Schmid factor of 0.45 (Scott and Orr, 1983). Representative experimental data points in Fig. 8(a), corresponding to an axial compressive strain rate of $\dot{\varepsilon} = 8.7 \times 10^{-6}$/s, display serrations associated with load drops that correlate with fast twin nucleation, propagation, and broadening (Scott and Orr, 1983). In Fig. 8(a), ε is the nominal total axial strain and τ is the resolved shear stress acting on a twin system. Model predictions in Fig. 8(a) correspond to $\tau = \overline{g}^j = g_S^j$ computed via (55). Because no slip systems are active, (60) does not result in any hardening associated with forest dislocations accumulated during slip, so the present model provides a constant twin resistance at a given temperature. The model correctly predicts a lower twin resistance at the higher temperature observed in experiments at higher strains ($\varepsilon > 0.12$), but does not predict the converse behavior at lower strains. It is noted that present use of (60) with parameters in Table 5 is at the upper limit of validity, with regards to temperature, of the fit shown in Fig. 5 for rhombohedral twinning because shear stresses required for rhombohedral twinning do not decrease significantly as the temperature is increased above 1200 K (Scott and Orr, 1983; Castaing et al., 2002). The model (at 1173 K) bounds most experimental data in Fig. 8(a) from above, but does not capture undulations in stress–strain behavior associated in experiments with sequential activation and fast propagation of individual twins within a single crystal. Some such undulations are artifacts of the limited velocity of the testing machine (Scott and Orr, 1983; Castaing et al., 2002).

Basal slip followed by rhombohedral twinning is considered quantitatively in Fig. 8(b). Boundary conditions applicable to Fig. 8(b) are explained by Castaing et al. (2002): a single crystal is compressed in uniaxial stress applied along the *ab* direction, at an angle of 57° from [0001] in the $(1\overline{2}10)$ plane, in two stages. In the first stage, the temperature is held at $\theta = 1567$ K, which favors basal slip (two systems each with Schmid factor of 0.4), presuming, as noted above, that stress needed for rhombohedral twinning does not decrease significantly above 1200 K (Scott and Orr, 1983; Castaing et al., 2002). The specimen is then cooled to $\theta = 1169$ K. In the second stage, the crystal is reloaded in compression along the same direction, which at this lower temperature, favors rhombohedral twinning (two systems with a Schmid factor of 0.15) because basal slip resistance increases significantly with decreasing temperature. Model predictions for axial stress σ (positive
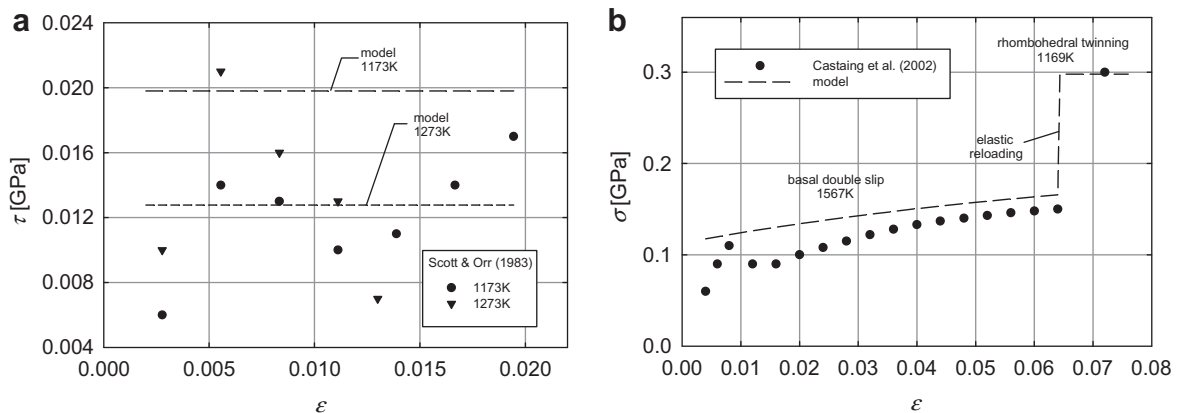

Fig. 8. Resolved shear stresses for rhombohedral twinning in pure alumina (a) and axial compressive stress for basal double slip followed by rhombohedral twinning (see text) in pure alumina (b).

in compression) are compared with experimental results in Fig. 8(b). The first loading stage activates double basal slip, and simultaneously leads to hardening of rhombohedral twin systems via (60). After elastic reloading, the second stage activates rhombohedral twinning on two possible systems. The experiment (Castaing et al., 2002), performed at a strain rate of $\dot{\varepsilon} = 2 \times 10^{-5}$/s, was apparently terminated after first occurrence of twinning. The model predicts constant twin resistance stress as twinning progresses in the second stage. From Fig. 8(b), the model over-predicts the saturation stress for basal double slip by 10–20% (recall that parameters used in (57) and (58) and listed in Table 5 are calibrated independently to single slip data), but the rhombohedral twin resistance after basal slip appears to be accurately modeled.

Hardening of prism and pyramidal slip and basal twinning systems by dislocation accumulation have not been quantified but could be addressed by straightforward extension of (57)–(60). Potential twin–twin interactions, hardening of slip systems within twins, and hardening of slip by twinning also remain to be quantified for pure and doped alumina.

Stored elastic energies of dislocation lines (energy per unit length) and twin boundaries (energy per unit area) are written

$$E_\rho = \frac{\mu b^2}{4\pi K} \ln\left(\frac{R}{R_C}\right) + \widehat{E} \approx \frac{\kappa_1 \mu b^2}{2}, \quad E_T = \frac{W_{SF}}{2} \approx \frac{\kappa_2 \mu b}{2}, \tag{61}$$

where in the first of (61), K accounts for the edge or screw character of the dislocation line as well as elastic anisotropy (Eshelby, 1949; Foreman, 1955), R is the radial distance from the dislocation core, R_C is the cut-off radius for the dislocation core, and $\widehat{E}$ is a correction that accounts for the core energy, line curvature, interaction energies from other defects and boundaries, and stacking faults associated with partial slip dislocations. As a first approximation (Hull and Bacon, 1984; Heuer et al., 1998), $\kappa_1 = 2.0/K$ is assumed. The value of K depends upon the orientation of the dislocation line with respect to the anisotropic crystal lattice (Foreman, 1955; Steeds, 1973); for large numbers of dislocation orientations, it becomes prudent to use isotropic approximations $K = 1$ for screw dislocations and $K = 1 - \nu$ for edge dislocations. Recall from Section 3.4 and Table 4 that $W_{SF} \approx 0.25 - 10$ J/m^2 is a typical stacking fault energy associated with twin systems in alumina, from which κ_2 in residual energy (46) and (61) can be estimated as $W_{SF}/(\mu b)$. Kenway, 1993 suggested that the variation in stacking fault energy with temperature in alumina is small, i.e., $\partial W_{SF}/\partial \theta \approx -1.1 \times 10^{-4}$ J/(m^{2}K).

Consider now the residual elastic energy accumulated in the crystal during single slip at constant temperature. From (61), the cumulative value β of dissipation fraction β' in (50) is approximated as

$$\beta = \left(\int \overline{g}^i d\gamma^i - \mu b^2 \rho_T / K \right) \left(\int \overline{g}^i d\gamma^i \right)^{-1} \quad \text{(single slip)}. \tag{62}$$

Predicted dissipation fraction β is shown in Fig. 9(a) for pure sapphire deformed at various temperatures, and in Fig. 9(b) for doped alumina single crystals deformed at approximately 1800 K. In each case, β is computed via integration of (57) and use of (59), (62), and material parameters listed in Tables 5 and 6. Since during experiments (Pletka et al., 1977, 1982) dislocations of families with various Burgers vectors and line orientations were generated, in the computations the representative value used for b is the rhombohedral lattice parameter and used for μ the rhombohedral shear modulus. Shown are results for edge dislocations and screw dislocations; in corundum, energy storage ratio $1 - \beta$ differs by a factor of $K = 0.76$ between these two kinds of dislocations. In the experiments, curved lines and loops were also observed, whose energies are only approximated by straight line formula in the first of (61). At all temperatures, the stored energy appears fairly small relative to the plastic work, since $\beta > 0.75$, in agreement with observed trends for many engineering metals (Taylor and Quinney, 1934; Clayton, 2005).
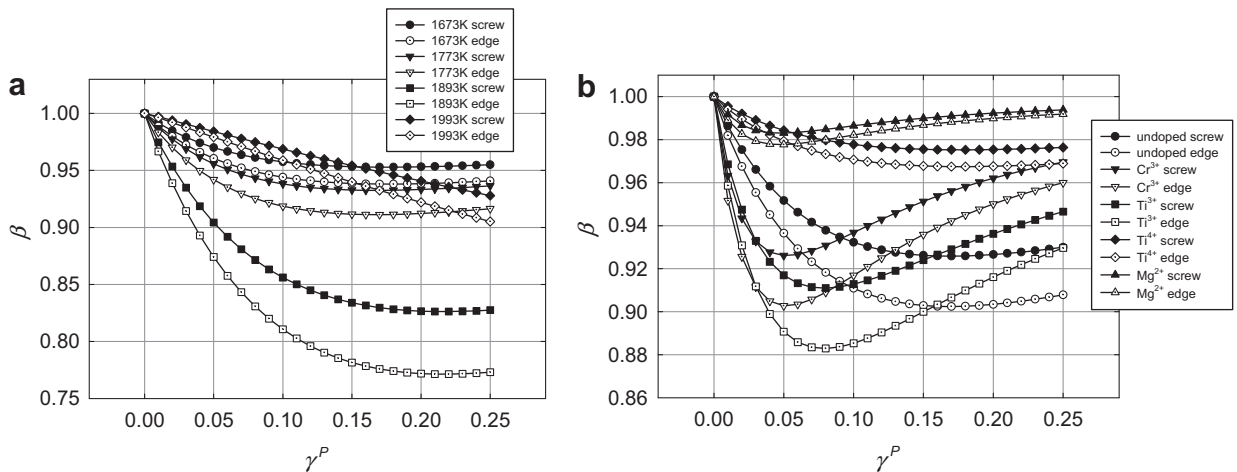

Fig. 9. Predicted cumulative heat dissipation fraction from slip on the basal plane: (a) pure alumina over range of temperatures and (b) pure and doped alumina at $\theta \approx 1800$ K.

It is noted that (61) and (62) account for dislocation interactions only in an approximate way, via choice of the empirical proportionality constant $\kappa_1 = 2.0/K$ (Hull and Bacon, 1984; Heuer et al., 1998). Specifically, the energy per unit volume of dislocations is assumed proportional to their total line length per unit volume, i.e., energy/volume = energy/length× length/volume = $E_\rho \times \rho_T = (\mu b^2/K) \times \rho_T$, with proportionality constant E_ρ assumed fixed at a given temperature. As demonstrated later in Section 4.5 and Table 8, the computed value of $E_\rho = 46.3$ nJ/m for full edge dislocations on the basal plane at null temperature from (61) is very close to the value from atomic simulations (Bodur et al., 2005), $E_\rho = 47.4$ nJ/m at a dislocation density $\rho_T \approx 10^{12}$ m^{-2} representative of the application in Figs. 6, 7 and 9. A more detailed approach accounting for differences in dislocation interaction energies at different dislocation densities would enable a possibly nonlinear relationship between dislocation density and defect energy per unit volume.

Consider next the energy of twin boundaries. Geometric arguments can be applied to demonstrate that the area of twin boundaries per unit volume of lamellar twins is approximately

$$\eta_T = 2 \sum_{j=1}^{w} f^j/t^j, \tag{63}$$

where t^j is the mean thickness of a twin comprising fraction j with volume fraction f^j. A proportionality relationship between characteristic twin thickness and twin volume fraction was also proposed by Proust et al. (2007). For propagation of a single twin system, the analog of (62) is

$$\beta = \left(\int \overline{g}^j \gamma^j df^j - E_T \eta_T \right) \left(\int \overline{g}^j \gamma^j df^j \right)^{-1} = 1 - W_{SF} \left(t^j \gamma^j \overline{g}^j \right)^{-1} \quad \text{(single twin system)}, \tag{64}$$

where $\overline{g}^j$ is assumed here only a function of temperature, and the second of (61) is used. Ranges of thickness spanning 0.1 μm $\leqslant t^j \leqslant 500$ μm for basal and rhombohedral twins in sapphire have been reported (Heuer, 1966; Scott and Orr, 1983; Inkson, 2000; Castaing et al., 2004). From (64), dissipation factor β increases with increasing thickness, twinning shear, and twinning stress, and decreases with increasing stacking fault energy. Considering rhombohedral twins (twinning shear $\gamma^j = 0.202$), a minimum thickness of 0.1 μm, a maximum stacking fault energy of 10 J/m^2, and the twin resistance provided by the second of (55) and Table 5, (64) gives a lower bound of $\beta > 0.999$ for $0 \leqslant \theta \leqslant 2100$ K. Hence, omission of the pure twin boundary contribution to the ratio of stored to dissipated energy appears to be a reasonable assumption in crystal plasticity modeling of alumina. However, interaction energies between twins and dislocations could still be tangible and may merit consideration via nonzero κ_4 and κ_6 in (46)–(48).

4.4. Residual volume changes

Residual volume change $\overline{J}$ was introduced in Section 3, following (3), (4) and (12). An estimation of this quantity from nonlinear elasticity theory is (Zener, 1942; Seeger and Haasen, 1958; Teodosiu, 1982; Clayton and Bammann, 2009)

$$\overline{J} - 1 = \frac{\Delta V}{V_0} = \frac{1}{B} \left(\frac{\partial B}{\partial p} - 1 \right) \overline{W}_D + \frac{1}{G} \left(\frac{\partial G}{\partial p} - \frac{G}{B} \right) \overline{W}_S, \tag{65}$$

where G and B are isotropic shear and bulk moduli, $p = -\text{tr}\boldsymbol{\sigma}/3$ is the Cauchy pressure, and $\overline{W}_D$ and $\overline{W}_S$ are dilatational and deviatoric strain energy densities per unit volume, respectively, arising from microscopic elastic fields of defects within a volume element of crystal. Volume change in (65) is measured between reference and intermediate configurations: $\Delta V = \overline{V} - V_0$ with $\overline{V}$ the volume in $\overline{B}$. Partitioning the elastic energies per unit dislocation line length in the first of (61) into dilatational and deviatoric parts, (65) can be written as (Seeger and Haasen, 1958; Teodosiu, 1982)

$$\overline{J} - 1 = \frac{\Delta V}{V_0} = \begin{cases} \frac{1}{3K} \left[\frac{1-\nu-2\nu^2}{(1-\nu)B} \left(\frac{\partial B}{\partial p} - 1 \right) + \frac{2-2\nu+2\nu^2}{(1-\nu)G} \left(\frac{\partial G}{\partial p} - \frac{G}{B} \right) \right] E_\rho \rho_T \text{ (edge)}, \\ \frac{1}{G} \left(\frac{\partial G}{\partial p} - \frac{G}{B} \right) E_\rho \rho_T \text{ (screw)}, \end{cases} \tag{66}$$

with $E_\rho = \mu b^2 (4\pi K)^{-1} \ln(R/R_C) \approx \mu b^2/K$. Closed form expressions for residual elastic volume change exist only for single crystals of isotropic or cubic symmetry (Toupin and Rivlin, 1960; Clayton and Bammann, 2009), and have been applied in analysis of volume changes from stored energy of cold work in metal polycrystals (Wright, 1982). An exact solution for the residual elastic volume change, and possibly shape change, in a highly anisotropic (e.g., trigonal) Bravais lattice would require integration over local elastic displacement gradients induced by defects within the body (Toupin and Rivlin, 1960; Clayton and Bammann, 2009), though simpler methods of approximation of volume changes based on thermodynamic arguments exist (Zener, 1942; Holder and Granato, 1969). Here, following previous studies (Seeger and Haasen, 1958), the isotropic approximation (66) is investigated as an order-of-magnitude estimate, consistent with the isotropic approximation of dislocation energies in (61). Formal derivations and limitations of (65) and (66) are discussed by Clayton and Bammann (2009).

Table 7 shows values of the normalized volume change $\Delta V/(Lb^2)$, where L is the total length of dislocation lines of pure screw or pure edge character, and b is the magnitude of the Burgers vector. For alumina, effective isotropic constants (Holm et al., 1999 and Appendix C) and their pressure derivatives (Sarkar et al., 1996) are obtained from the literature. Values of the

normalized volume change in Al_2O_3 from dislocation lines are positive in agreement with other solids (Seeger and Haasen, 1958; Wright, 1982), are very to close those for metallic crystal Cu (face centered cubic), and are $\sim 2/3$ of those for ionic crystal NaCl (cubic rock salt). Data for residual volume changes and dislocation densities are available for Cu polycrystals (Clarebrough et al., 1957); the range of values for the volume change per line length in the rightmost column of Table 7 corresponds to applied compressive strains ranging from 0.3 to 0.7 and dislocation line densities found from energy measurements. The theory thus provides reasonably accurate results for Cu, within a factor of two of the experimental values.

Shown in Fig. 10(a) are volume changes computed from (66) and properties in Table 7, for distributions of pure edge and pure screw dislocations of line densities predicted by the model in Fig. 7(a) for basal slip at various temperatures. Shown in Fig. 10(b) are volume changes computed from (66) and the properties in Table 7, for dislocations in pure and doped alumina of line densities predicted by the model in Fig. 7(b) for basal slip at $\theta \approx 1800$ K. At fixed temperature and composition, the predicted ratio of residual expansion in alumina for pure screw dislocations to that for pure edge dislocations is ≈ 0.6. As demonstrated by Clayton and Bammann (2009), the volume change for a crystal containing a mixture of non-interacting edge and screw dislocations would fall between predictions for densities of pure edge and pure screw dislocations. Volume changes remain small as saturation levels of dislocation density observed in high temperature basal glide are approached: $\Delta V/V_0 \approx 10^{-5}$ corresponds to the volume increase that would result from thermal expansion in alumina from a temperature rise of ≈ 0.7 K.

According to the theory, volume increases on the order of 1% would be achieved upon generation dislocation densities $\rho_T \approx 10^{16}$ m^{-2}, corresponding to a dislocation spacing on the order of 10 nm. Conceivably, very large dislocation densities may be required to enable extremely large plastic strain rates in shock physics experiments (Rohatgi and Vecchio, 2002) if the upper bound on dislocation velocity is limited to the velocity of transverse acoustic waves (Kocks et al., 1975). Densities $\rho_T \approx 10^{16}$ m^{-2} have been approached in such cases (Merala et al., 1988; Rohatgi and Vecchio, 2002). Generation of defect densities of this magnitude could affect the measured pressure–volume response; for example, the pressure required to offset a 1% volume increase would be on the order of $0.01B \approx 2.5$ GPa. However, it is noted that the approximations in (61) and (66) may decrease in validity as dislocation spacings decrease and interaction energies among dislocations become stronger. Atomic simulations offer the possibility of more accurate predictions of effects of large defect densities on volume changes, effective (tangent) elastic moduli, and stored energies (Dienes, 1952; Bodur et al., 2005; Chung and Clayton, 2007).

Table 7
Effective isotropic elastic properties and volume changes associated with dislocations.

Crystal	G [GPa]	B [GPa]	v	$\partial G/\partial p$	$\partial B/\partial p$	$\Delta V/(Lb^2)$ edge	$\Delta V/(Lb^2)$ screw	$\Delta V/(Lb^2)$ experiment[c]
Al_2O_3[a]	157	250	0.24	1.7	4.2	1.7	1.0	–
NaCl[b]	15	23	0.24	2.0	5.8	2.5	1.4	–
Cu[b]	47	152	0.36	1.2	5.6	1.8	1.0	1.6–2.3

[a] Sarkar et al. (1996) and Holm et al. (1999).
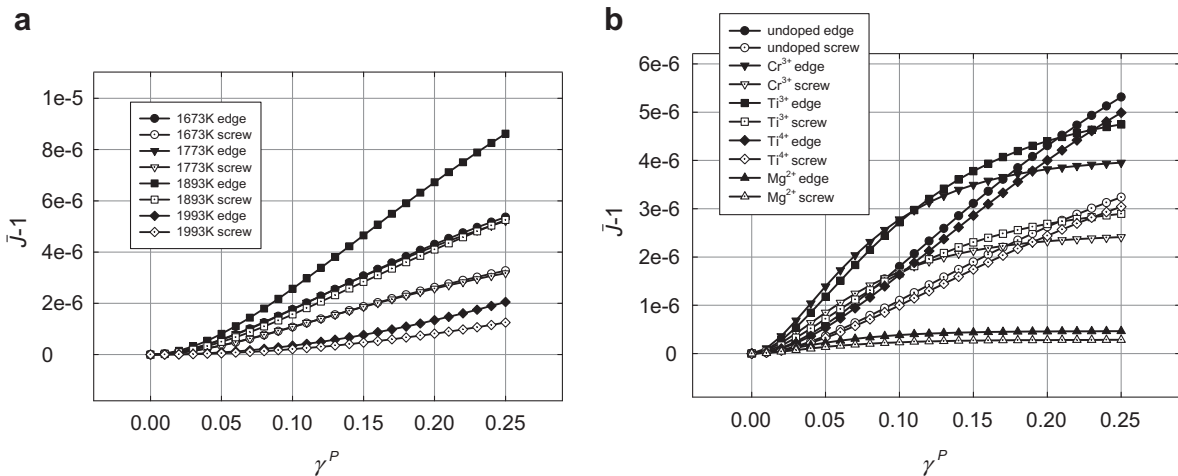[b] Seeger and Haasen (1958).
[c] Clarebrough et al. (1957).

Fig. 10. Predicted volume changes resulting from dislocation lines accumulated during slip on the basal plane: (a) pure alumina over range of temperatures and (b) pure and doped alumina at $\theta \approx 1800$ K.

For example, Bodur et al. (2005) reported a decrease in energy per unit length E_ρ of periodically arranged edge dislocation dipoles on the basal plane by about a factor of 3, from 47 4 nJ/m (Table 8) to 16.5 nJ/m, as the dislocation density is increased from $\rho_T \approx 10^{12}$ m^2 to $\rho_T \approx 10^{16}$ m^{-2}. Accounting for this decrease, the volume increase computed via (66) at a large dislocation density of $\rho_T \approx 10^{16}$ m^{-2} would be reduced by a factor of 3, to about 0.3%, corresponding to a pressure change on the order of 0.8 GPa. A procedure for computing residual volume changes (as well as possible shape changes) associated with defects in a self-equilibrated lattice in terms of anharmonic contributions to inter-atomic potentials is outlined by Clayton and Bammann (2009).

Finally consider volume changes attributed to twin boundaries (i.e., appropriate stacking fault energies) bounded according to the second of (61) and (65) as

$$\frac{1}{2G}\left(\frac{\partial G}{\partial p} - \frac{G}{B}\right)W_{SF}\eta_T \leqslant \frac{\Delta V}{V_0} \leqslant \frac{1}{2B}\left(\frac{\partial B}{\partial p} - 1\right)W_{SF}\eta_T. \tag{67}$$

Holder and Granato (1969) suggested that the lower bound in (67) would be appropriate for low-angle grain boundaries constructed from arrays of screw dislocations. Using values from Table 7 for elastic constants and their pressure derivatives, and using a maximum stacking fault energy of 10 J/m^2, (67) becomes $3.4 \times 10^{-11}\eta_T \leqslant \Delta V/V_0 \leqslant 6.4 \times 10^{-11}\eta_T$, with the area per unit volume of twin boundaries η_T in dimensions of m^{-1}. From (63), with $f^j = 1$ and a minimum twin thickness $t^j = 0.1$ μm (Inkson, 2000), bounds for the volume change are $6.8 \times 10^{-6} \leqslant \Delta V/V_0 \leqslant 1.3 \times 10^{-5}$. Comparing with results in Fig. 10, this maximum volume change from the stored energy of twin boundaries is of the same order of magnitude as that predicted from dislocation lines accumulated in single crystals of corundum at high temperatures at shear strains on the order of 0.25. Not considered here are possible effects of doping on elastic coefficients, which could be important if doping alters the concentration of vacancies or interstitials (Dienes, 1952).

4.5. Comparison with atomic calculations

In Table 8, parameters or predictions of the present model are compared with results of atomic calculations published elsewhere or with theoretical models. The initial resistance to slip of basal dislocations of the present model in (55) is compared to values obtained from molecular dynamics (MD) simulations of hypervelocity impact (Zhang et al., 2007, 2008) and consideration of the generalized stacking fault energy gradient (Nishimura et al., 2009) using MD simulations as well as quantum mechanics (density functional theory or DFT). Also shown are values of the theoretical Peierls–Nabarro stress (Peierls, 1940; Clayton, 2009) for full edge and screw dislocations on the basal plane. The value of initial slip resistance for the present model at null temperature, 12.7 GPa, falls between Peierls–Nabarro stresses for edge and screw dislocations, and is ~ 15–35% lower than the atomic simulation results. It is noted that the present model does not incorporate effects of hydrostatic pressure on the basal slip resistance. Extremely high pressures generated during hypervelocity impact (Zhang et al., 2008) or indentation (Tymiak and Gerberich, 2007) could conceivably cause an increase in the apparent glide (as well as twinning) resistance, as has been noted in MD simulations of other materials (Xu et al., 2004). For example, if the glide resistance is assumed proportional to the shear modulus (Peierls, 1940; Nabarro, 1947; Kocks et al., 1975), at a pressure of 100 GPa, the shear modulus and hence the glide resistance would approximately double in magnitude over its value at ambient pressure, if the pressure derivative of the shear modulus, 1.7 in Table 7, sufficiently describes the variation of shear modulus up to such pressures. In previous work (Clayton, 2009), the lower value of 4.3 GPa at room temperature was found to provide a reasonable explanation for possible occurrence of basal slip in plate impact experiments on single crystals (Graham and Brooks, 1971) at lower pressures on the order of 10–20 GPa.

Table 8
Comparison of model features with atomic or theoretical calculations.

Quantity	Present model		Atomic/theoretical calculation	
	Value	Equation	Value	Reference
Basal glide resistance g_S^i	12.7 GPa (0 K)	(55)	15 GPa	[a]
	4.3 GPa (300 K)	(55)	16.3 GPa (MD)	[b]
			18.9 GPa (DFT)	[b]
			9.6 GPa (edge, 0 K)	[c]
			17.9 GPa (screw, 0 K)	[c]
Basal dislocation energy E_ρ	46.3 nJ/m (edge, 0 K)	(61)	47.4 nJ/m (edge, 0 K)	[d]
	35.2 nJ/m (screw, 0 K)	(61)		
Basal stacking fault dilatancy $(\Delta V/V)/\eta_T$	0.028–0.052 nm	(67)	0.028–0.096 nm	[e]

[a] Zhang et al. (2007, 2008).
[b] Nishimura et al. (2009).
[c] Peierls (1940) and Nabarro (1947).
[d] Bodur et al. (2005).
[e] Marinopoulos and Elsasser (2001).

The energy per unit length of full dislocations on the basal plane obtained using (61) with $\kappa_1 = 2/K$ and $\mu = C_{44}$ is compared in Table 8 with results of MD simulations of full basal plane edge dislocations (Bodur et al., 2005). The edge dislocation energy agrees closely with the atomic calculation, the latter valid for a dislocation line density of $\approx 10^{12}$ m^{-2} (Bodur et al., 2005) in the null temperature limit.

In the final row of Table 8, the volume increase from basal plane stacking faults computed using the bounds in (67) is compared with results of molecular simulations (Marinopoulos and Elsasser, 2001). Specifically, the volume change per density of stacking faults is computed in (67) using a representative stacking fault energy $W_{SF} = 4.0$ J/m^2, multiplied by a factor of two because here η_T represents the stacking fault density rather than the twin boundary density. Atomic simulation results follow from consideration of computed expansions normal to various kinds of basal plane stacking faults ranging in magnitude from 5.5% to 18.7% of the rhombohedral lattice parameter a_0, computed for relaxed structures at null external pressure and null temperature (Marinopoulos and Elsasser, 2001). Basal plane stacking faults are associated with partial dislocations of type $1/3\langle 10\bar{1}0 \rangle\{0001\}$, which only involve the cation (i.e., Al) sub-lattice, since $1/3\langle 10\bar{1}0 \rangle$ is a perfect translation vector in the anion (i.e., O) sub-lattice. Agreement between the present model and the quoted atomic calculations is reasonable. Dilatancy for various relaxed stacking fault structures on basal and prism planes was also computed by Kenway (1993).

5. Conclusions

Anisotropic mechanisms of elasticity, plastic slip, and twinning have been addressed in a crystal plasticity model with consistent thermodynamics. Finite deformation theory is required for addressing large shears arising from slip and twinning, lattice reorientation arising from twinning, and nonlinear elastic effects. Accordingly, each mechanism has been represented explicitly within a multiplicative decomposition of the deformation gradient. A constitutive framework with internal state variables provides thermodynamic relationships among state variables and driving forces for time rates of inelastic deformations. Internal state variables consist of geometrically necessary and statistically stored dislocation densities, twin boundary area densities, and twinned volume fractions. Dissipative inelastic deformation rates consist of rates of plastic shear, rates of twin fractions, and rates of volume changes attributed to defect content. The present theoretical model extends that of previous work (Clayton, 2009) by its explicit incorporation of geometrically necessary dislocations corresponding to gradients of inelastic stretch and rotation and statistically stored dislocations associated with dislocation dipoles and closed loops. Kinematic identities demonstrate the contributions of slip and twinning to the geometrically necessary dislocation density tensor (e.g., full, partial, and interfacial dislocations). Both geometrically necessary and statistically stored dislocations are addressed in the thermodynamic framework.

A fully nonlinear, anisotropic, crystal plasticity model for mechanical and thermodynamic behavior of pure and doped corundum has been developed and exercised, accounting for lattice defects mentioned above, i.e., dislocation densities, twin boundary densities, and twinned volume fractions. Specific inelastic deformation modes include basal, prism, and pyramidal slip and basal and rhombohedral twinning. Hardening from dislocation accumulation during basal slip has been quantified in pure and doped corundum single crystals, and stored energies associated with dislocations and twin boundaries have been estimated. The cumulative ratio of stored energy from dislocations to dissipated energy in basal slip is predicted at less than 25% for plastic shears of less than 0.25 and temperatures greater than 1600 K, regardless of dopant concentration. Upon consideration of stacking fault energies and twin thicknesses observed in sapphire, stored energies associated exclusively with twin boundaries appear orders of magnitude smaller than those of dislocation lines. Volumetric expansions from nucleation of dislocation lines and twin boundaries have been estimated using formulae originating from nonlinear elasticity theory (Clayton and Bammann, 2009, and references therein). Such expansions are predicted small in alumina for dislocation line densities observed in low pressure, high temperature experiments (Pletka et al., 1977, 1982), and are also predicted small for twin boundaries of spacing (Inkson, 2000) and energy (Lagerlof et al., 1984) observed experimentally. New predictions for rhombohedral twinning, including hardening by prior basal slip, are provided; these predictions offer a reasonable depiction of experimental results (Scott and Orr, 1983; Castaing et al., 2002). Finally, model features pertinent to defects on the basal plane are compared with atomic calculations. Expansion associated with stacking faults predicted via the nonlinear elastic approach of the present theory compares favorably with predictions of atomic simulations (Marinopoulos and Elsasser, 2001).

Appendix A

Isochoric characteristics of twinning and slip noted in (12) are derived in what follows. The Jacobian determinant of the deformation gradient in (2) is computed as (Truesdell and Toupin, 1960; Eringen, 1962; Marsden and Hughes, 1983)

$$J = \sqrt{\frac{\det \mathbf{g}}{\det \mathbf{G}}} \det \mathbf{F} = \frac{1}{6}\varepsilon_{abc}\varepsilon^{ABC}F^a_{\cdot A}F^b_{\cdot B}F^c_{\cdot C}, \tag{A1}$$

where by notational convention, determinants of metric tensors $\mathbf{g}$ and $\mathbf{G}$ are absorbed into permutation tensors ε_{abc} and ε^{ABC}, respectively. It follows that (Ericksen, 1960; Thurston, 1974)

$$\frac{\partial J}{\partial F^a_{\cdot A}} = \frac{1}{6}\varepsilon_{bcd}\varepsilon^{BCD}\frac{\partial}{\partial F^a_{\cdot A}}(F^b_{\cdot B}F^c_{\cdot C}F^d_{\cdot D}) = \frac{1}{6}\varepsilon_{bcd}\varepsilon^{BCD}(\delta^A_{\cdot B}\delta^b_{\cdot a}F^c_{\cdot C}F^d_{\cdot D} + \delta^A_{\cdot C}\delta^c_{\cdot a}F^b_{\cdot B}F^d_{\cdot D} + \delta^A_{\cdot D}\delta^d_{\cdot a}F^b_{\cdot B}F^c_{\cdot C})$$

$$= \frac{1}{6}(\varepsilon_{cda}\varepsilon^{CDA}F^c_{\cdot C}F^d_{\cdot D} + \varepsilon_{dba}\varepsilon^{DBA}F^d_{\cdot D}F^b_{\cdot B} + \varepsilon_{bca}\varepsilon^{BCA}F^b_{\cdot B}F^c_{\cdot C}) = \frac{1}{2}\varepsilon_{cda}\varepsilon^{CDA}F^c_{\cdot C}F^d_{\cdot D} = \frac{1}{6}\varepsilon_{cda}\varepsilon^{CDA}F^c_{\cdot C}F^d_{\cdot D}\delta^E_{\cdot E}$$

$$= \frac{1}{6}\varepsilon_{cda}\varepsilon^{CDA}F^c_{\cdot C}F^d_{\cdot D}F^e_{\cdot E}F^{-1E}_{\cdot e} = \frac{1}{6}\varepsilon_{cde}\varepsilon^{CDE}F^c_{\cdot C}F^d_{\cdot D}F^e_{\cdot E}F^{-1A}_{\cdot a} = JF^{-1A}_{\cdot a}. \tag{A2}$$

To verify the final two equalities in (A2), notice that $JF^{-1A}_{\cdot a}F^a_{\cdot A} = 3J = (1/2)\varepsilon_{cda}\varepsilon^{CDA}F^c_{\cdot C}F^d_{\cdot D}F^a_{\cdot A}$. The material time derivative of (A1) is computed as follows using the chain rule, noting that material time derivatives of metric tensors vanish for stationary coordinate systems (Eringen, 1962):

$$\dot{J} = \frac{\partial J}{\partial F^a_{\cdot A}}\dot{F}^a_{\cdot A} = JF^{-1A}_{\cdot a}\dot{F}^a_{\cdot A} = J\dot{F}^a_{\cdot A}F^{-1A}_{\cdot a} = JL^a_{\cdot a} = J\mathrm{tr}\mathbf{L}, \tag{A3}$$

where $\mathbf{L}$ is the spatial velocity gradient of (8). Applying the same arguments to J^I of (4),

$$J^I = \frac{1}{6}\varepsilon_{\alpha\beta\chi}\varepsilon^{\delta\varepsilon\phi}F^{I\alpha}_{\cdot\delta}F^{I\beta}_{\cdot\varepsilon}F^{I\chi}_{\cdot\phi}, \tag{A4}$$

$$\frac{\partial J^I}{\partial F^{I\alpha}_{\cdot\beta}} = J^I F^{I-1\beta}_{\cdot\alpha}, \tag{A5}$$

$$\dot{J}^I = \frac{\partial J^I}{\partial F^{I\alpha}_{\cdot\beta}}\dot{F}^{I\alpha}_{\cdot\beta} = J^I F^{I-1\beta}_{\cdot\alpha}\dot{F}^{I\alpha}_{\cdot\beta} = J^I\dot{F}^{I\alpha}_{\cdot\beta}F^{I-1\beta}_{\cdot\alpha} = J^I L^{I\alpha}_{\cdot\alpha} = J^I\mathrm{tr}\mathbf{L^I}, \tag{A6}$$

with $\mathbf{L^I}$ defined in (9) and (10). From (5) and (10),

$$\dot{J}^I = J^I\mathrm{tr}\mathbf{L^I} = J^I\mathrm{tr}\left(\sum_{j=1}^w\dot{f}^j\gamma^{ij}\mathbf{\bar{s}}^j_0\otimes\mathbf{\overline{m}}^j_0\right) = J^I\sum_{j=1}^w\dot{f}^j\gamma^{ij}\underbrace{\mathbf{\bar{s}}^j_0\cdot\mathbf{\overline{m}}^j_0}_{=0} = 0. \tag{A7}$$

Since by definition, $J^I(t=0) = 1$, (A7) yields the isochoric conditions

$$J^I = 1(\forall t \geqslant 0). \tag{A8}$$

Now consider the product $\mathbf{\widehat{F}} = \mathbf{F^I}\mathbf{F^P}$. The following equalities apply:

$$\widehat{J} = J^I J^P = \frac{1}{6}\varepsilon_{\alpha\beta\chi}\varepsilon^{ABC}\widehat{F}^\alpha_{\cdot A}\widehat{F}^\beta_{\cdot B}\widehat{F}^\chi_{\cdot C}, \tag{A9}$$

$$\frac{\partial\widehat{J}}{\partial\widehat{F}^\alpha_{\cdot A}} = \widehat{J}\widehat{F}^{-1A}_{\cdot\alpha}, \tag{A10}$$

$$\dot{\widehat{J}} = \frac{\partial\widehat{J}}{\partial\widehat{F}^\alpha_{\cdot A}}\dot{\widehat{F}}^\alpha_{\cdot A} = \widehat{J}\widehat{F}^{-1A}_{\cdot\alpha}\dot{\widehat{F}}^\alpha_{\cdot A} = \widehat{J}\dot{\widehat{F}}^\alpha_{\cdot A}\widehat{F}^{-1A}_{\cdot\alpha} = \widehat{J}\mathrm{tr}(\dot{\mathbf{F}}^\mathbf{I}\mathbf{F}^{\mathbf{I}-1} + \mathbf{F^I}\dot{\mathbf{F}}^\mathbf{P}\mathbf{F}^{\mathbf{P}-1}\mathbf{F}^{\mathbf{I}-1}) = J^I J^P\mathrm{tr}(\mathbf{L^I} + \mathbf{\overline{L}^P}), \tag{A11}$$

where definitions in (9) have been used. Applying the product rule to (A9) and using (A7) and (A8) in (A11) gives

$$\dot{\widehat{J}} = \underbrace{\dot{J}^I}_{=0}J^P + \underbrace{J^I}_{=1}\dot{J}^P = \dot{J}^P = \underbrace{J^I}_{=1}J^P(\underbrace{\mathrm{tr}\mathbf{L^I}}_{=0} + \mathrm{tr}\mathbf{\overline{L}^P}) = J^P\mathrm{tr}\mathbf{\overline{L}^P}. \tag{A12}$$

Now taking the trace of (11) and using (5) and (6), (A12) reduces to

$$\dot{J}^P = J^P\mathrm{tr}\mathbf{\overline{L}^P} = J^P\mathrm{tr}\left[(1-f_T)\sum_{i=1}^n\dot{\gamma}^i\mathbf{\bar{s}}^i_0\otimes\mathbf{\overline{m}}^i_0 + \sum_{j=1}^w\left(f^j\sum_{i=1}^n\dot{\gamma}^i_j\mathbf{\bar{s}}^i_{0j}\otimes\mathbf{\overline{m}}^i_{0j}\right)\right]$$

$$= J^P\left[(1-f_T)\sum_{i=1}^n\dot{\gamma}^i\mathbf{\bar{s}}^i_0\cdot\mathbf{\overline{m}}^i_0 + \sum_{j=1}^w\left(f^j\sum_{i=1}^n\dot{\gamma}^i_j\mathbf{\bar{s}}^i_{0j}\cdot\mathbf{\overline{m}}^i_{0j}\right)\right] \tag{A13}$$

$$= J^P(1-f_T)\sum_{i=1}^n\dot{\gamma}^i\underbrace{\mathbf{\bar{s}}^i_0\cdot\mathbf{\overline{m}}^i_0}_{=0} + J^P\sum_{j=1}^w\left(f^j\sum_{i=1}^n\dot{\gamma}^i_j\underbrace{(\mathbf{\overline{Q}}^j\mathbf{s}^i_0)\cdot(\mathbf{m}^i_0\mathbf{\overline{Q}}^{jT})}_{=0}\right) = 0.$$

Since by definition, $J^P(t=0) = 1$, (A13) yields

$$J^P = 1(\forall t \geqslant 0). \tag{A14}$$

Appendix B

An alternative to multiplicative decomposition (3) in which the sequence of $\mathbf{F^I}$ and $\mathbf{F^P}$ is reversed is considered in what follows. It is demonstrated that the sequence of $\mathbf{F^I}$ and $\mathbf{F^P}$ in the multiplicative decomposition does not significantly affect other aspects of the theoretical model of Section 3.

Decomposition (3) is replaced with

$$\mathbf{F} = \mathbf{F^E}\bar{J}^{1/3}\mathbf{F^P}\mathbf{F^I} = \mathbf{F^E}\overline{\mathbf{F}} = \mathbf{F^L}\widehat{\mathbf{F}}, \quad \mathbf{F^L} = \mathbf{F^E}\bar{J}^{1/3}, \quad \widehat{\mathbf{F}} = \mathbf{F^P}\mathbf{F^I}. \tag{B1}$$

Jacobian determinants of deformation mappings in (4) are instead

$$J = \sqrt{\frac{\det \mathbf{g}}{\det \mathbf{G}}} \det \mathbf{F} = J^E\bar{J}J^PJ^I, \quad J^E = \sqrt{\det \mathbf{g}}\det \mathbf{F^E}, \quad J^P = \det \mathbf{F^P}, \quad J^I = \sqrt{\frac{1}{\det \mathbf{G}}}\det \mathbf{F^I}. \tag{B2}$$

Spatial velocity gradient (8) is replaced with

$$\mathbf{L} = \dot{\mathbf{F}}\mathbf{F}^{-1} = \dot{\mathbf{F}}^E\mathbf{F}^{E-1} + \mathbf{F^E}\dot{\mathbf{F}}^P\mathbf{F}^{P-1}\mathbf{F}^{E-1} + \mathbf{F^E}\mathbf{F^P}\dot{\mathbf{F}}^I\mathbf{F}^{I-1}\mathbf{F}^{P-1}\mathbf{F}^{E-1} + (1/3)\dot{\bar{J}}\bar{J}^{-1}\mathbf{1}. \tag{B3}$$

Inelastic velocity gradient (9) is instead

$$\dot{\overline{\mathbf{F}}}\overline{\mathbf{F}}^{-1} = \dot{\mathbf{F}}^P\mathbf{F}^{P-1} + \mathbf{F^P}\dot{\mathbf{F}}^I\mathbf{F}^{I-1}\mathbf{F}^{P-1} + (1/3)\dot{\bar{J}}\bar{J}^{-1}\mathbf{1} = \mathbf{L^P} + \overline{\mathbf{L}}^I + (1/3)\dot{\bar{J}}\bar{J}^{-1}\mathbf{1}, \tag{B4}$$

where the following definitions apply instead of (10) and (11):

$$\overline{\mathbf{L}}^I = \mathbf{F^P}\dot{\mathbf{F}}^I\mathbf{F}^{I-1}\mathbf{F}^{P-1} = \sum_{j=1}^{w} \dot{f}^j\gamma^j\overline{\mathbf{s}}_0^j \otimes \overline{\mathbf{m}}_0^j, \tag{B5}$$

$$\mathbf{L^P} = (1 - f_T)\sum_{i=1}^{n} \dot{\gamma}^i\overline{\mathbf{s}}_0^i \otimes \overline{\mathbf{m}}_0^i + \sum_{j=1}^{w}\left(f^j\sum_{i=1}^{n}\dot{\gamma}_j^i\overline{\mathbf{s}}_{0j}^i \otimes \overline{\mathbf{m}}_{0j}^i\right). \tag{B6}$$

As a consequence of (B5) and (B6), and similarly to (12), twinning and slip are always isochoric:

$$\mathrm{tr}\overline{\mathbf{L}}^I = \mathrm{tr}\mathbf{L^P} = 0 \Rightarrow \dot{J}^I = \dot{J}^P = 0 \Rightarrow J^I = J^P = 1 \quad (t \geqslant 0), \tag{B7}$$

so that the first of (B2) reduces to $J = J^E\bar{J} = J^L$. The total Burgers vector associated with geometrically necessary defects in (13) is replaced with

$$B^\alpha = -\int_C \widehat{F}_{.A}^\alpha dX^A = -\int_C F_{.\beta}^{P\alpha}F_{.A}^{I\beta} dX^A = \int_A \alpha_G^{\alpha A} N_A dA, \tag{B8}$$

where the two-point dislocation density tensor of (14) is instead

$$\alpha_G^{\alpha A} = \underbrace{\varepsilon^{ABC}F_{.B}^{I\beta}F_{.\beta,C}^{P\alpha}}_{\text{slip gradients}} + \underbrace{\varepsilon^{ABC}F_{.\beta}^{P\alpha}F_{.B,C}^{I\beta}}_{\text{twin gradients}}. \tag{B9}$$

The geometrically necessary dislocation tensor $\hat{\boldsymbol{\alpha}}$ following the second and third equalities of (15) is unchanged. The treatment of constitutive behavior, thermodynamics, and kinetics in Sections 3.2–3.5 is unchanged except that $\mathbf{L}^I$ is replaced with $\overline{\mathbf{L}}^I$ of (B5) and $\overline{\mathbf{L}}^P$ is replaced with $\mathbf{L^P}$ of (B6). Notice that the right sides of (B5) and (B6) are, by assumption, identical to right sides of (10) and (11), respectively, so that $\dot{\overline{\mathbf{F}}}\overline{\mathbf{F}}^{-1}$ is computed identically in terms of slip and twin system activity regardless of the sequence of $\mathbf{F^I}$ and $\mathbf{F^P}$ in the decomposition of $\mathbf{F}$.

Appendix C

The shear elastic constant μ entering free energy contribution (46) can be prescribed in a number of ways for anisotropic materials. When the energy of lattice defects is dominated by a single prominent family of dislocations, μ should be chosen consistently with κ_1 to yield the correct energy per unit length of dislocation line. Various solutions for the energy factor for dislocations in anisotropic crystals are given by Foreman (1955), Steeds (1973). When different kinds of dislocations, stacking faults, and twin boundaries affect the energy as in (46), μ is simply viewed as an effective (isotropic) elastic shear modulus, and coefficients $\kappa_1, \kappa_2, \ldots \kappa_6$ then scale the energy associated with each kind of defect in an appropriate manner.

A number of averaging or self-consistent methods are available for computation of effective elastic constants (Hill, 1952; Sarkar et al., 1996). Perhaps the most common is the Voigt average (Hill, 1952):

$$\mu_V = \frac{1}{15}\left[(C_{11} + C_{22} + C_{33}) - (C_{12} + C_{23} + C_{13}) + 3(C_{44} + C_{55} + C_{66})\right], \tag{C1}$$

$$B_V = \frac{1}{9}\left[C_{11} + C_{22} + C_{33} + 2(C_{12} + C_{23} + C_{13})\right], \tag{C2}$$

where μ_V and B_V are, respectively, Voigt-averaged shear and bulk moduli that provide an upper bound to the true effective elastic constants of an isotropic polycrystal. For sapphire, noting that for a trigonal crystal $C_{11} = C_{22}, C_{13} = C_{23}, C_{44} = C_{55}$, and $C_{66} = (1/2)(C_{11} - C_{12})$ (Thurston, 1974), (C1) and (C2) yield $\mu_V = 166$ GPa and $B_V = 255$ GPa. Various experimental and theoretically computed values of isotropic shear and bulk moduli quoted by Holm et al. (1999) for α-alumina fall in the range 156 GPa $\leqslant G \leqslant$ 166 GPa and 245 GPa $\leqslant B \leqslant$ 255 GPa, with effective Poisson's ratio 0.23 $\leqslant v \leqslant$ 0.24.

For calculations in Sections 4.2 and 4.3 of the present paper that focus primarily on basal slip, $\mu = C_{44}$ has been used, since this is considered an appropriate shear elastic coefficient for basal slip, and since $\mu(\theta = 0\ \text{K}) = 156$ GPa (Table 2) produces a value of energy per unit length of basal plane edge dislocations consistent with that predicted by atomic simulations (Table 8). For calculations of Section 4.4 of the present paper that rely on isotropic shear and bulk moduli (Table 7), representative values of $B = 250$ GPa and $v = 0.24$ have been used (Holm et al., 1999), leading to effective isotropic shear modulus $G = 3B(1 - 2v)/(2 + 2v) = 157$ GPa.

References

Abu Al-Rub, R.K., Voyiadjis, G.Z., 2004. Analytical and experimental determination of the material intrinsic length scale of strain gradient plasticity theory from micro- and nano-indentation experiments. Int. J. Plast. 20, 1139–1182.

Arsenlis, A., Parks, D.M., 1999. Crystallographic aspects of geometrically-necessary and statistically-stored dislocation density. Acta Mater. 47, 1597–1611.

Asaro, R.J., 1983. Crystal plasticity. ASME J. Appl. Mech. 50, 921–934.

Ashby, M.F., 1970. The deformation of plastically non-homogeneous media. Philos. Mag. 21, 399–424.

Bammann, D.J., 2001. A model of crystal plasticity containing a natural length scale. Mater. Sci. Eng. A, 406–410.

Beltz, G.E., Rice, J.R., Shih, C.F., Xia, L., 1996. A self-consistent model for cleavage in the presence of plastic flow. Acta Metall. 44, 3943–3954.

Bernstein, N., Tadmor, E.B., 2004. Tight-binding calculations of stacking energies and twinnability in fcc metals. Phys. Rev. B 69, 094116.

Beyerlein, I.J., Tomé, C.N., 2008. A dislocation-based constitutive law for pure Zr including temperature effects. Int. J. Plast. 24, 867–895.

Bhattacharya, K., 1991. Wedge-like microstructure in martensites. Acta Metall. Mater. 39, 2431–2444.

Bilby, B.A., Crocker, A.G., 1965. The theory of the crystallography of deformation twinning. Proc. R. Soc. Lond. A 288, 240–255.

Bilby, B.A., Gardner, L.R.T., Stroh, A.N., 1957. Continuous distributions of dislocations and the theory of plasticity. In: Proc. 9th Int. Congr. Appl. Mech. Bruxelles, vol. 8, pp. 35–44.

Bodur, C.T., Chang, J., Argon, A.S., 2005. Molecular dynamics simulations of basal and pyramidal system edge dislocations in sapphire. J. Eur. Ceram. Soc. 25, 1431–1439.

Born, M., Huang, K., 1954. Dynamical Theory of Crystal Lattices. Oxford University Press, Oxford.

Bourne, N.K., 2006. Impact on alumina. I. Response at the mesoscale. Proc. R. Soc. Lond. A 462, 3061–3080.

Bourne, N.K., Gray III, G.T., 2002. On the failure of shocked titanium diboride. Proc. R. Soc. Lond. A 458, 1273–1284.

Bourne, N.K., Millett, J.C.F., Chen, M., McCauley, J.W., Dandekar, D.P., 2007. On the Hugoniot elastic limit in polycrystalline alumina. J. Appl. Phys. 102, 073514.

Brugger, K., 1964. Thermodynamic definition of higher order elastic coefficients. Phys. Rev. 133, A1611–A1612.

Burghartz, S., Schulz, B., 1994. Thermophysical properties of sapphire, AlN, and MgAl2O4 down to 70 K. J. Nucl. Mater. 212, 1065–1068.

Cahill, D.G., Lee, S.M., Selinder, T.I., 1998. Thermal conductivity of κ-Al2O3 and α-Al2O3 wear-resistant coatings. J. Appl. Phys. 83, 5783–5786.

Castaing, J., Cadoz, J., Kirby, S.H., 1981. Prismatic slip of Al2O3 single crystals below 1000 °C in compression under hydrostatic pressure. J. Am. Ceram. Soc. 64, 504–511.

Castaing, J., Munoz, A., Dominguez Rodriguez, A., 2002. Hardening of rhombohedral twinning in sapphire (α-Al2O3) by basal slip dislocations. Philos. Mag. A 82, 1419–1431.

Castaing, J., He, A., Lagerlof, K.P.D., Heuer, A.H., 2004. Deformation of sapphire (α-Al2O3) by basal slip and basal twinning below 700 °C. Philos. Mag. 84, 1113–1125.

Castanet, R., 1984. Selected data on the thermodynamic properties of α-alumina. High Temp. High Press. 16, 449–457.

Chang, R., 1960. Creep of Al2O3 single crystals. J. Appl. Phys. 31, 484–487.

Chin, G.Y., Hosford, W.F., Mendorf, D.R., 1969. Accommodation of constrained deformation in FCC metals by slip and twinning. Proc. R. Soc. Lond. A 309, 433–456.

Christian, J.W., Mahajan, S., 1995. Deformation twinning. Prog. Mater. Sci. 39, 1–157.

Chung, P.W., Clayton, J.D., 2007. Multiscale modeling of point and line defects in cubic lattices. Int. J. Multiscale Comput. Eng. 5, 203–226.

Clarebrough, L.M., Hargreaves, M.E., West, G.W., 1957. The density of dislocations in compressed copper. Acta Metall. 5, 738–740.

Clayton, J.D., 2005. Dynamic plasticity and fracture in high density polycrystals: constitutive modeling and numerical simulation. J. Mech. Phys. Solids 53, 261–301.

Clayton, J.D., 2009. A continuum description of nonlinear elasticity, slip, and twinning, with application to sapphire. Proc. R. Soc. Lond. A 465, 307–334.

Clayton, J.D., Bammann, D.J., 2009. Finite deformations and internal forces in elastic–plastic crystals: interpretations from nonlinear elasticity and anharmonic lattice statics. ASME J. Eng. Mater. Tech. 131, 041201.

Clayton, J.D., McDowell, D.L., 2003. A multiscale multiplicative decomposition for elastoplasticity of polycrystals. Int. J. Plast. 19, 1401–1444.

Clayton, J.D., Bammann, D.J., McDowell, D.L., 2004a. A multiscale gradient theory for elastoviscoplasticity of single crystals. Int. J. Eng. Sci. 42, 427–457.

Clayton, J.D., Bammann, D.J., McDowell, D.L., 2004b. Anholonomic configuration spaces and metric tensors in finite elastoplasticity. Int. J. Nonlinear Mech. 39, 1039–1049.

Clayton, J.D., Bammann, D.J., McDowell, D.L., 2005. A geometric framework for the kinematics of crystals with defects. Philos. Mag. 85, 3983–4010.

Clayton, J.D., McDowell, D.L., Bammann, D.J., 2006. Modeling dislocations and disclinations with finite micropolar elastoplasticity. Int. J. Plast. 22, 210–256.

Clayton, J.D., Chung, P.W., Grinfeld, M.A., Nothwang, W.D., 2008. Kinematics, electromechanics, and kinetics of dielectric and piezoelectric crystals with lattice defects. Int. J. Eng. Sci. 46, 10–30.

Coleman, B.D., Gurtin, M.E., 1967. Thermodynamics with internal state variables. J. Chem. Phys. 17, 597–613.

Cousins, C.S.G., 1978. Inner elasticity. J. Phys. C 11, 4867–4879.

Dienes, G.J., 1952. A theoretical estimate of the effect of radiation on the elastic constants of simple metals. Phys. Rev. 86, 228–234.

Eckart, C., 1948. The thermodynamics of irreversible processes IV. The theory of elasticity and anelasticity. Phys. Rev. 73, 373–382.

El-Dasher, B.S., Adams, B.L., Rollett, A.D., 2003. Viewpoint: experimental recovery of geometrically necessary dislocation density in polycrystals. Scr. Metall. 48, 141–145.

Ericksen, J.L., 1960. Tensor fields. In: Flugge, S. (Ed.), Handbuch der Physik, vol. III/1. Springer-Verlag, Berlin, pp. 794–858.

Ericksen, J.L., 1984. The Cauchy and Born hypothesis for crystals. In: Gurtin, M.E. (Ed.), Phase Transformations and Material Instabilities in Solids. Academic Press, pp. 61–78.

Eringen, A.C., 1962. Nonlinear Theory of Continuous Media. McGraw-Hill, New York.

Eshelby, J.D., 1949. Edge dislocations in anisotropic materials. Philos. Mag. 40, 903–912.

Eshelby, J.D., 1975. The elastic energy-momentum tensor. J. Elast. 5, 321–335.

Farber, Y.A., Yoon, S.Y., Lagerlof, K.P.D., Heuer, A.H., 1993. Microplasticity during high temperature indentation and the Peierls potential of sapphire (α-Al$_2$O$_3$) single crystals. Phys. Status Solidi A 137, 485–498.

Fleck, N.A., Muller, G.M., Ashby, M.F., Hutchinson, J.W., 1994. Strain gradient plasticity: theory and experiment. Acta Metall. Mater. 42, 475–487.

Foreman, A.J.E., 1955. Dislocation energies in anisotropic crystals. Acta Metall. 3, 322–330.

Friedel, J., 1964. Dislocations. Pergamon, Oxford.

Geipel, T., Lagerlof, K.P.D., Pirouz, P., Heuer, A.H., 1994. A zonal dislocation mechanism for rhombohedral twinning in sapphire (α-Al$_2$O$_3$). Acta Metall. Mater. 42, 1367–1372.

Gilman, J.J., 1979. Resistance to shock-front propagation in solids. J. Appl. Phys. 50, 4059–4064.

Graham, R.A., Brooks, W.P., 1971. Shock-wave compression of sapphire from 15 to 420 kbar. The effects of large anisotropic compressions. J. Phys. Chem. Solids 32, 2311–2330.

Heuer, A.H., 1966. Deformation twinning in corundum. Philos. Mag. 13, 379–393.

Heuer, A.H., Lagerlof, K.P.D., Castaing, J., 1998. Slip and twinning dislocations in sapphire (α-Al$_2$O$_3$). Philos. Mag. A 78, 747–763.

Hill, R., 1952. The elastic behaviour of a crystalline aggregate. Proc. Phys. Soc. A 65, 349–354.

Hirth, J.P., Lothe, J., 1982. Theory of Dislocations. John Wiley and Sons, New York.

Holder, J., Granato, A.V., 1969. Thermodynamic properties of solids containing defects. Phys. Rev. 182, 729–741.

Holm, B., Ahuja, R., Yourdshahyan, Y., Johansson, B., Lundqvist, B.I., 1999. Elastic and optical properties of α- and κ-Al$_2$O$_3$. Phys. Rev. B 59, 12777–12787.

Hughes, D.A., Hansen, N., Bammann, D.J., 2003. Geometrically necessary boundaries, incidental dislocation boundaries, and geometrically necessary dislocations. Scr. Metall. 48, 147–153.

Hull, D., Bacon, D.J., 1984. Introduction to Dislocations, third ed. Butterworth-Heinemann, Oxford.

Hutchinson, J.W., 1976. Bounds and self-consistent estimates for creep of polycrystalline materials. Proc. R. Soc. Lond. A 348, 101–127.

Inkson, B.J., 2000. Dislocations and twinning activated by the abrasion of Al$_2$O$_3$. Acta Mater. 48, 1883–1895.

James, R.D., 1981. Finite deformation by mechanical twinning. Arch. Ration. Mech. Anal. 77, 143–176.

Kalidindi, S.R., 1998. Modeling the strain hardening response of low SFE FCC alloys. Int. J. Plast. 14, 1265–1277.

Kalidindi, S.R., 2001. Modeling anisotropic strain hardening and deformation textures in low stacking fault energy fcc metals. Int. J. Plast. 17, 837–860.

Kenway, P.R., 1993. Calculated stacking fault energies in α-Al$_2$O$_3$. Philos. Mag. B 68, 171–183.

Klassen-Neklyudova, M.V., Govorkov, V.G., Urusovskaya, A.A., Voinova, N.N., Kozlovskaya, E.P., 1970. Plastic deformation of corundum single crystals. Phys. Status Solidi 39, 679–688.

Kocks, U.F., Argon, A.S., Ashby, M.F., 1975. Thermodynamics and kinetics of slip. Prog. Mater. Sci. 19, 1–288.

Kratochvil, J., 1972. Finite strain theory of inelastic behavior of crystalline solids. In: Sawczuk, A. (Ed.), Foundations of Plasticity. Noordhoff, Leyden, pp. 401–415.

Kronberg, M.L., 1957. Plastic deformation of single crystals of sapphire: basal slip and twinning. Acta Metall. 5, 507–524.

Kuhlmann-Wildsorf, D., 1960. Frictional stress acting on a moving dislocation in an otherwise perfect crystal. Phys. Rev. 120, 773–781.

Lagerlof, K.P.D., Mitchell, T.E., Heuer, A.H., Riviere, J.P., Cadoz, J., Castaing, J., Phillips, D.S., 1984. Stacking fault energy in sapphire (α-Al$_2$O$_3$). Acta Metall. 32, 97–105.

Lagerlof, K.P.D., Heuer, A.H., Castaing, J., Riviere, J.P., Mitchell, T.E., 1994. Slip and twinning in sapphire (α-Al$_2$O$_3$). J. Am. Ceram. Soc. 77, 385–397.

Lankford, J., Predebon, W.W., Staehler, J., Subhash, G., Pletka, B., Anderson, C., 1998. The role of plasticity as a limiting factor in the compressive failure of high strength ceramics. Mech. Mater. 29, 205–218.

Lebensohn, R., 1999. Modelling the role of local correlations in polycrystal plasticity using viscoplastic self-consistent schemes. Modell. Simul. Mater. Sci. Eng. 7, 739–746.

Lebensohn, R.A., Tomé, C., 1993. A self-consistent anisotropic approach for the simulation of plastic deformation and texture development of polycrystals: application to zirconium alloys. Acta Metall. Mater. 41, 2611–2624.

Lee, Y.J., Subhash, G., Ravichandran, G., 1999. Constitutive modeling of textured body-centered-cubic (bcc) polycrystals. Int. J. Plast. 15, 625–645.

Lu, W.Y., Horstemeyer, M.F., Korellis, J.S., Grishabar, R.B., Mosher, D., 1998. High temperature sensitivity of notched AISI 304L stainless steel tests. Theor. Appl. Fract. Mech. 30, 139–152.

Mandel, J., 1974. Thermodynamics and plasticity. In: Delgado, J.J. (Ed.), Foundations of Continuum Thermo-Dynamics. Macmillan, New York, pp. 283–304.

Marinopoulos, A.G., Elsasser, C., 2001. Density-functional and shell-model calculations of the energetics of basal-plane stacking faults in sapphire. Philos. Mag. Lett. 81, 329–338.

Marsden, J.E., Hughes, T.J.R., 1983. Mathematical Foundations of Elasticity. Prentice-Hall, Englewood Cliffs.

Maugin, G.A., 1994. Eshelby stress in elastoplasticity and ductile fracture. Int. J. Plast. 10, 393–408.

Mayeur, J.R., McDowell, D.L., 2007. A three-dimensional crystal plasticity model for duplex Ti–6Al–4V. Int. J. Plast. 23, 1457–1485.

McCabe, R.J., Proust, G., Cerreta, E.K., Misra, A., 2009. Quantitative analysis of deformation twinning in zirconium. Int. J. Plast. 25, 454–472.

McDowell, D.L., 2005. Internal state variable theory. In: Yip, S. (Ed.), Handbook of Materials Modeling. Springer, The Netherlands, pp. 1151–1169.

McDowell, D.L., 2008. Viscoplasticity of heterogeneous metallic materials. Mater. Sci. Eng. R 62, 67–123.

McDowell, D.L., Moosbrugger, J.C., 1992. Continuum slip foundations of elasto-viscoplasticity. Acta Mech. 93, 73–87.

Merala, T.B., Chan, H.W., Howitt, D.G., 1988. Dislocation microstructures in explosively deformed hard materials. Mater. Sci. Eng. A, 293–298.

Nabarro, F.R.N., 1947. Dislocations in a simple cubic lattice. Proc. Phys. Soc. 59, 256–272.

Neil, C.J., Agnew, S.R., 2009. Crystal plasticity-based forming limit prediction for non-cubic metals: application to Mg alloy AZ31B. Int. J. Plast. 25, 379–398.

Nishimura, K., Chen, H.–P., Kalia, R.K., Nakano, A., Nomura, K., Vashishta, P., Shimojo, F., 2009. Response to "Comment on 'nanoindentation hardness anisotropy of alumina crystal: a molecular-dynamics study'". Appl. Phys. Lett. 94, 146102.

Nye, J.F., 1953. Some geometrical relations in dislocated crystals. Acta Metall. 1, 153–162.

Paul, H., Morawiec, A., Driver, J.H., Bouzy, E., 2009. On twinning and shear banding in a Cu-8 at.% Al alloy plane strain compressed at 77 K. Int. J. Plast. 25, 1588–1608.

Peierls, R.E., 1940. The size of a dislocation. Proc. Phys. Soc. 52, 34–37.

Pletka, B.J., Heuer, A.H., Mitchell, T.E., 1977. Work-hardening in sapphire (α-Al$_2$O$_3$). Acta Metall. 25, 25–33.

Pletka, B.J., Mitchell, T.E., Heuer, A.H., 1982. Dislocation substructures in doped sapphire (α-Al$_2$O$_3$) deformed by basal slip. Acta Metall. 30, 147–156.

Proust, G., Tomé, C.N., Kaschner, G.C., 2007. Modeling texture, twinning and hardening evolution during deformation of hexagonal materials. Acta Mater. 55, 2137–2148.

Proust, G., Tomé, C.N., Jain, A., Agnew, S.R., 2009. Modeling the effect of twinning and detwinning during strain-path changes of magnesium alloy AZ31. Int. J. Plast. 25, 861–880.

Rajendran, A.M., 1994. Modeling the impact behavior of AD85 ceramic under multiaxial loading. Int. J. Impact Eng. 15, 749–768.

Regueiro, R.A., Bammann, D.J., Marin, E.B., Garikipati, K., 2002. A nonlocal phenomenological anisotropic finite deformation plasticity model accounting for dislocation defects. ASME J. Eng. Mater. Tech. 124, 380–387.

Rezvanian, O., Zikry, M.A., Rajendran, A.M., 2007. Statistically stored, geometrically necessary and grain boundary dislocation densities: microstructural representation and modelling. Proc. R. Soc. Lond A 463, 2833–2853.

Rodriguez, M.C., Castaing, J., Munoz, A., Veyssiere, P., Rodriguez, A.D., 2008. Analysis of a kink pair model applied to a Peierls mechanism in basal and prism plane slips in sapphire (α-Al$_2$O$_3$) deformed between 200 and 1800 °C. J. Am. Ceram. Soc. 91, 1612–1617.

Rohatgi, A., Vecchio, K.S., 2002. The variation of dislocation density as a function of the stacking fault energy in shock-deformed FCC materials. Mater. Sci. Eng. A 328, 256–266.

Sarkar, S., Ballabh, T.K., Middya, T.R., Basu, A.N., 1996. T-matrix approach to effective nonlinear elastic constants of heterogeneous materials. Phys. Rev. B 54, 3926–3931.

Scheidler, M., Wright, T.W., 2001. A continuum framework for finite viscoplasticity. Int. J. Plast. 17, 1033–1085.

Schoenfeld, S.E., Kad, B., 2002. Texture effects on shear response in Ti–6Al–4V plates. Int. J. Plast. 18, 461–486.

Schouten, J.A., 1954. Ricci Calculus. Springer-Verlag, Berlin.

Scott, W.D., Orr, K.K., 1983. Rhombohedral twinning in alumina. J. Am. Ceram. Soc. 66, 27–32.

Seeger, A., Haasen, P., 1958. Density changes of crystals containing dislocations. Philos. Mag. 3, 470–475.

Shiekhelsouk, M.N., Favier, V., Inal, K., Cherkaoui, M., 2009. Modelling the behaviour of polycrystalline austenitic steel with twinning-induced plasticity effect. Int. J. Plast. 25, 105–133.

Smith, A.D.N., 1953. The effects of small amounts of cold work on Young's modulus of copper. Philos. Mag. A 44, 453–466.

Snow, J.D., Heuer, A.H., 1973. Slip systems in Al_2O_3. J. Am. Ceram. Soc. 56, 153–157.

Staroselsky, A., Anand, L., 2003. A constitutive model for hcp materials deforming by slip and twinning: application to magnesium alloy AZ31B. Int. J. Plast. 19, 1843–1864.

Steeds, J.W., 1973. Introduction to Anisotropic Elasticity Theory of Dislocations. Clarendon Press, Oxford.

Taheri, M., Weiland, H., Rollett, A., 2006. A method of measuring stored energy macroscopically using statistically stored dislocations in commercial purity aluminum. Metall. Mater. Trans. A 37, 19–25.

Taylor, G.I., 1934. The mechanism of plastic deformation of crystals. Proc. R. Soc. Lond. A 145, 362–415.

Taylor, G.I., Quinney, H., 1934. The latent energy remaining in a metal after cold working. Proc. R. Soc. Lond. A 143, 307–326.

Teodosiu, C. 1970. A dynamic theory of dislocations and its applications to the theory of the elastic–plastic continuum. In: Simmons, J.A., De Wit, R., Bullough, R. (Eds.), Fundamental Aspects of Dislocation Theory. U.S. Nat. Bur. Stand. Spec. Pub. 317, vol. II, pp. 837–876.

Teodosiu, C., 1982. Elastic Models of Crystal Defects. Springer-Verlag, Berlin.

Teodosiu, C., Sidoroff, F., 1976. A finite theory of the elastoviscoplasticity of single crystals. Int. J. Eng. Sci. 14, 713–723.

Thamburaja, P., Pan, H., Chau, F.S., 2009. The evolution of microstructure during twinning: constitutive equations, finite-element simulations and experimental verification. Int. J. Plast. 25, 2141–2168.

Thurston, R.N., 1974. Waves in solids. In: Truesdell, C. (Ed.), Handbuch der Physik, vol. VIa/4. Springer-Verlag, Berlin, pp. 109–308.

Tomé, C., Lebensohn, R.A., Kocks, U.F., 1991a. A model for texture development dominated by deformation twinning: application to zirconium alloys. Acta Metall. Mater. 39, 2667–2680.

Tomé, C.N., Wenk, H.-R., Canova, G.R., Kocks, U.F., 1991b. Simulations of texture development in calcite: comparison of polycrystal plasticity theories. J. Geophys. Res. 96, 11865–11875.

Toupin, R.A., Rivlin, R.S., 1960. Dimensional changes in crystals caused by dislocations. J. Math. Phys. 1, 8–15.

Tressler, R.E., Barber, D.J., 1974. Yielding and flow of *c*-axis sapphire filaments. J. Am. Ceram. Soc. 57, 13–19.

Truesdell, C.A., Toupin, R.A., 1960. The classical field theories. In: Flugge, S. (Ed.), Handbuch der Physik, vol. III/1. Springer-Verlag, Berlin, pp. 226–793.

Tymiak, N.I., Gerberich, W.W., 2007. Initial stages of contact-induced plasticity in sapphire. I. Surface traces of slip and twinning. Philos. Mag. 87, 5143–5168.

Tymiak, N., Chrobak, D., Gerberich, W., Warren, O., Nowak, R., 2009. Role of competition between slip and twinning in nanoscale deformation of sapphire. Phys. Rev. B 79, 174116.

Van Houtte, P., 1978. Simulation of the rolling and shear texture of brass by the Taylor theory adapted for mechanical twinning. Acta Metall. 26, 591–604.

Veit, K., 1921. Artificial deformations and transpositions in minerals. Neues Jahrb. Miner. 45, 121–148.

Voyiadjis, G.Z., Abu Al-Rub, R.K., 2007. Nonlocal gradient-dependent thermodynamics for modeling scale-dependent plasticity. Int. J. Multiscale Comput. Eng. 5, 295–323.

Willis, J.R., 1967. Second-order effects of dislocations in anisotropic crystals. Int. J. Eng. Sci. 5, 171–190.

Winey, J.M., Gupta, Y.M., Hare, D.E., 2001. *R*-axis sound speed and elastic properties of sapphire single crystals. J. Appl. Phys. 90, 3109–3111.

Wright, T.W., 1982. Stored energy and plastic volume change. Mech. Mater. 1, 185–187.

Wu, X., Kalidindi, S.R., Necker, C., Salem, A.A., 2007. Prediction of crystallographic texture evolution and anisotropic stress-strain curves during large plastic strains in high purity α-titanium using a Taylor-type crystal plasticity model. Acta Mater. 55, 423–432.

Xu, D.-S., Chang, J.-P., Li, J., Yang, R., Li, D., Yip, S., 2004. Dislocation slip or deformation twinning: confining pressure makes a difference. Mater. Sci. Eng. A, 840–844.

Zanzotto, G., 1996. The Cauchy–Born hypothesis, nonlinear elasticity, and mechanical twinning in crystals. Acta Crystallogr. A 52, 839–849.

Zener, C., 1942. Theory of lattice expansion introduced by cold work. Trans. Am. Inst. Min. Metall. Eng. 147, 361–368.

Zhang, K.S., Wu, M.S., Feng, R., 2005. Simulation of microplasticity-induced deformation in uniaxially strained ceramics by 3-D Voronoi polycrystal modeling. Int. J. Plast. 21, 801–834.

Zhang, C., Kalia, R.K., Nakano, A., Vashishta, P., 2007. Hypervelocity impact induced deformation modes in α-alumina. Appl. Phys. Lett. 91, 071906.

Zhang, C., Kalia, R.K., Nakano, A., Vashishta, P., Branicio, P.S., 2008. Deformation mechanisms and damage in α-alumina under hypervelocity impact loading. J. Appl. Phys. 103, 083508.

Zouboulis, E.S., Grimsditch, M., 1991. Refractive index and elastic properties of single-crystal corundum (α-Al_2O_3) up to 2100 K. J. Appl. Phys. 70, 772–776.

No. of Copies	Organization
1 ELEC	ADMNSTR DEFNS TECHL INFO CTR ATTN DTIC OCP 8725 JOHN J KINGMAN RD STE 0944 FT BELVOIR VA 22060-6218
1	US ARMY RSRCH LAB ATTN RDRL WMM B G GAZONAS ABERDEEN PROVING GROUND MD 21005
1	US ARMY RSRCH LAB ATTN RDRL WMP B C HOPPEL BLDG 393 ABERDEEN PROVING GROUND MD 21005
1	US ARMY RSRCH LAB ATTN RDRL WMP B D CASEM BLDG 4600 ABERDEEN PROVING GROUND MD 21005
16	US ARMY RSRCH LAB ATTN RDRL WMP B J CLAYTON (15 COPIES) ATTN RDRL WMP B M GREENFIELD ABERDEEN PROVING GROUND MD 21005
2	US ARMY RSRCH LAB ATTN RDRL WMP B T WEERASOORIYA ATTN RDRL WMP C T W BJERKE BLDG 4600 ABERDEEN PROVING GROUND MD 21005
1	US ARMY RSRCH LAB ATTN RDRL WMP F N GNIAZDOWSKI BLDG 390 ABERDEEN PROVING GROUND MD 21005
1	US ARMY RSRCH LAB ATTN RDRL WMP S E SCHOENFELD BLDG 393 ABERDEEN PROVING GROUND MD 21005

No. of Copies	Organization
1	US ARMY RSRCH LAB ATTN RDRL CIM G T LANDFRIED BLDG 4600 ABERDEEN PROVING GROUND MD 21005-5066
1	US ARMY RSRCH LAB ATTN RDRL WM J MCCAULEY BLDG 4600 ABERDEEN PROVING GROUND MD 21005-5069
3	US ARMY RSRCH LAB ATTN IMNE ALC HRR MAIL & RECORDS MGMT ATTN RDRL CIM L TECHL LIB ATTN RDRL CIM P TECHL PUB ADELPHI MD 20783-1197

TOTAL: 29 (1 ELEC, 28 HCS)

INTENTIONALLY LEFT BLANK.